NEUROSCIENCE

Proteomic signatures of corona and herpes viral antibodies identify IGDCC4 as a mediator of neurodegeneration

Michael R. Duggan[1]*, Shuojia Yang[2], Gabriela T. Gomez[3], Yuhan Cui[4], Ana W. Capuano[5], Jingsha Chen[6], Zhijian Yang[4], Junhao Wen[7,8,9,10], Guray Erus[4], Shannon M. Drouin[1], David Zweibaum[11], Qu Tian[11], Julián Candia[11], Murat Bilgel[1], Alexandria Lewis[3], Abhay Moghekar[3], Nicholas J. Ashton[12,13,14,15], Przemysław R. Kac[12], Thomas K. Karikari[12,16], Kaj Blennow[12,17,18,19], Henrik Zetterberg[12,17,20,21,22,23], Brion S. Maher[24,25], Adam P. Spira[24,25,26], Logan Dumitrescu[27,28], Timothy J. Hohman[27,28], Rebecca F. Gottesman[29], Christos Davatzikos[4], David A. Bennett[5], Josef Coresh[30], Luigi Ferrucci[11], Susan M. Resnick[1], Robert Yolken[2], Keenan A. Walker[1]

Mechanisms underlying the dynamic relationships of viral infections and neurodegeneration warrant examination. Using a community-based cohort of older adults, the current study characterized the neurocognitive (cognitive functioning, brain volumes, Alzheimer's disease positron emission tomography, and plasma biomarkers) and plasma proteomic (7268 proteins) profiles of four common coronavirus and six herpesvirus antibody titers. Genetic inference techniques demonstrated the associations between viral antibody titers and neurocognitive outcomes may be attributed to altered expression in a subset of mechanistically relevant proteins in plasma. One of these proteins, IGDCC4 (immunoglobulin superfamily deleted in colorectal cancer subclass member 4), was related to 20-year dementia risk, cognitive functioning, and amyloid-β positivity using data from two independent cohorts, while its plasma and intrathecal abundance were causally implicated in dementia risk and clinically relevant brain atrophy. Our findings illuminate the biological basis by which host immune responses to viruses may affect neurocognitive outcomes in older adults and identify IGDCC4 as an important molecular mediator of neurodegeneration.

INTRODUCTION

Systemic and central nervous system (CNS) immune processes play an important role in Alzheimer's disease (AD) and related dementias (ADRD) (*1*), but mechanisms underlying the dynamic relationships between viral infections and ADRD warrant further examination. Severe, hospitalized infections (e.g., sepsis and pneumonia) can increase ADRD risk, and we recently found that symptomatic viral infections can accelerate regional brain atrophy (*2*–*6*). On the other hand, serological assays of more common, often asymptomatic viral infections have shown variable results, including reports of lower ADRD risk and higher brain volumes among individuals with elevated antibody titers (*7*–*11*). Meanwhile, accumulating epidemiological evidence shows decreased ADRD risk following different types of viral vaccinations (*12*). While it is unlikely that viral infections exert protective effects on neurological disease, these patterns could suggest that individuals predisposed to mount a more robust immune response to viruses (i.e., higher antibody levels due to host genetic factors and/or differences in exposures) may also be less susceptible to neurodegeneration. However, the biological processes that may account for these relationships are unclear.

Viral antibody levels may be associated with unique circulating proteomes that can interact with target cells of the brain and influence its structure and function through a variety of mechanisms (*13*, *14*). For example, altered plasma concentrations of cytokines following severe

[1]Laboratory of Behavioral Neuroscience, National Institute on Aging, National Institutes of Health, Baltimore, MD, USA. [2]Stanley Laboratory of Neurovirology, Department of Pediatrics, Johns Hopkins University School of Medicine, Baltimore, MD, USA. [3]Department of Neurology, Johns Hopkins University School of Medicine, Baltimore, MD, USA. [4]Artificial Intelligence in Biomedical Imaging Laboratory, Perelman School of Medicine, University of Pennsylvania, Philadelphia, PA, USA. [5]Rush Alzheimer's Disease Center, Rush University Medical Center, Chicago, IL, USA. [6]Department of Epidemiology, Johns Hopkins University Bloomberg School of Public Health, Baltimore, MD, USA. [7]Laboratory of AI and Biomedical Science, Columbia University, New York, NY, USA. [8]New York Genome Center, New York, NY, USA. [9]Data Science Institute (DSI), Columbia University, New York, NY, USA. [10]Center for Innovation in Imaging Biomarkers and Integrated Diagnostics, Department of Radiology, Columbia University, New York, NY, USA. [11]Translational Gerontology Branch, National Institute on Aging, National Institutes of Health, Baltimore, MD, USA. [12]Department of Psychiatry and Neurochemistry, Institute of Neuroscience and Physiology, University of Gothenburg, Mölndal, Sweden. [13]Maurice Wohl Clinical Neuroscience Institute, King's College London, London, UK. [14]NIHR Biomedical Research Center for Mental Health and Biomedical Research Unit for Dementia at South London and Maudsley NHS Foundation, London, UK. [15]Center for Age-Related Medicine, Stavanger University Hospital, Stavanger, Norway. [16]Department of Psychiatry, School of Medicine, University of Pittsburgh, Pittsburgh, PA, USA. [17]Clinical Neurochemistry Laboratory, Sahlgrenska University Hospital, Mölndal, Sweden. [18]ICM Institute, Pitié-Salpêtrière University Hospital, Sorbonne University, Paris, France. [19]First Affiliated Hospital, University of Science and Technology of China, Anhui, China. [20]Department of Neurodegenerative Disease, University College London Institute of Neurology, London, UK. [21]UK Dementia Research Institute, University College London, London, UK. [22]Hong Kong Center for Neurodegenerative Diseases, Hong Kong, China. [23]Wisconsin Alzheimer's Disease Research Center, University of Wisconsin School of Medicine and Public Health, University of Wisconsin-Madison, Madison, WI, USA. [24]Department of Mental Health, Johns Hopkins Bloomberg School of Public Health, Baltimore, MD, USA. [25]Department of Psychiatry and Behavioral Sciences, Johns Hopkins School of Medicine, Baltimore, MD, USA. [26]Johns Hopkins Center on Aging and Health, Baltimore, MD, USA. [27]Vanderbilt Memory and Alzheimer's Center, Vanderbilt University Medical Center, Nashville, TN, USA. [28]Vanderbilt Genetics Institute, Vanderbilt University Medical Center, Nashville, TN, USA. [29]Stroke Branch, National Institute of Neurological Disorders and Stroke, Bethesda, MD, USA. [30]Departments of Population Health and Medicine, New York University Grossman School of Medicine, New York, NY, USA.
*Corresponding author. Email: dugganmr@nih.gov

acute respiratory syndrome coronavirus 2 (SARS-CoV-2) infection can affect cognition and brain volumes by engaging with cells along the blood-brain barrier (*15*). In addition, changes in the broader plasma proteome following other types of viral infections can influence dementia risk, brain atrophy, and ADRD biomarkers (*6*, *16*). The use of high-throughput proteomic platforms can enable these insights by identifying reliable, scalable predictors and determinants of neurodegeneration (*17*). Given their relatively high prevalence and reported associations with neurologic health (*18*, *19*), examining the plasma proteomic signatures of common coronavirus and herpesvirus antibodies may reveal specific molecular conduits that link host immune responses to neurodegeneration.

Using a community-based cohort of older adults from the Baltimore Longitudinal Study of Aging (BLSA), the current study characterized the neurocognitive and plasma proteomic profiles of four corona and six herpes virus antibody titers, including their associations with prevalent dementia, cognitive performance, brain volumes, positron emission tomography (PET) and plasma ADRD biomarkers, and the plasma proteome (7268 proteins). After identifying a subset of proteins differentially expressed with multiple titers, we demonstrated via two-sample Mendelian randomization (MR) that genetic variation modulating their abundance in plasma was mechanistically relevant to neurodegeneration. One of these proteins, IGDCC4 (immunoglobulin superfamily deleted in colorectal cancer subclass member 4), was associated with long-term incident dementia risk, cognitive functioning, and the presence of cortical amyloid-β (Aβ) using data from two independent cohorts. After demonstrating that genetic variation modulating IGDCC4's intrathecal abundance was mechanistically relevant to neurodegeneration, we analyzed the biological processes by which this protein might exert its downstream effects, including proximal protein interactions, enriched canonical pathways, and unique expression patterns (i.e., cell and tissue specific, AD patient and transgenic mouse brain tissue).

RESULTS

Coronavirus and herpesvirus antibodies are associated with lower odds of dementia, higher cognitive performance, and preserved regional brain volumes

Four coronavirus titers [human coronavirus (HCoV)–229E, HCoV-HKU1, HCoV-NL63, and HCoV-OC43) and six herpesvirus titers {Epstein-Barr virus (EBV) [EBV nuclear antigen (EBNA) and EBV capsid antigen (VCA)], herpes simplex virus type 1 (HSV-1), cytomegalovirus (CMV) [immunoglobulin G (IgG) and IgM], and varicella-zoster virus (VZV)} were measured in plasma of 323 BLSA participants [age = 77.6 years (SD = 10.1); 43.7% female; 78.3% white] (Fig. 1, fig. S1, and table S1). All measurements reflected IgGs, with the exception of CMV, where IgMs were also quantified. No participants maintained an active diagnosis (International Classification of Diseases, 9th Revision) of a coronavirus or herpesvirus infection, although 5.3% showed evidence of another infection type, most often a urinary tract infection (n = 5). Titer levels did not significantly differ by marriage status or household size (fig. S2), but did differ by coronavirus- and/or herpesvirus-related *HLA* variants identified in previous genome-wide association studies (GWAS) (table S2 and fig. S3), suggesting that variation in this sample's antibody levels may be related to host immune predispositions and not differences in community exposures. Titer levels did not vary by *APOEε4* genotype (table S2 and fig. S2). Standardized continuous titer measurements, their tertiles, and cumulative burden indices [i.e., percentage of measurements in the top tertiles of coronavirus, herpesvirus, and total (coronavirus and herpesvirus)] were examined as predictors of neurocognitive outcomes. Serostatus was not assessed, as older adults show that high rates of seropositivity and cut points among these individuals can be unreliable (*20*). All samples were collected before the SARS-CoV-2 pandemic, and we demonstrated that blood draws were evenly distributed across months and seasons to ensure that findings were not affected by seasonality (fig. S4). Cumulative burden

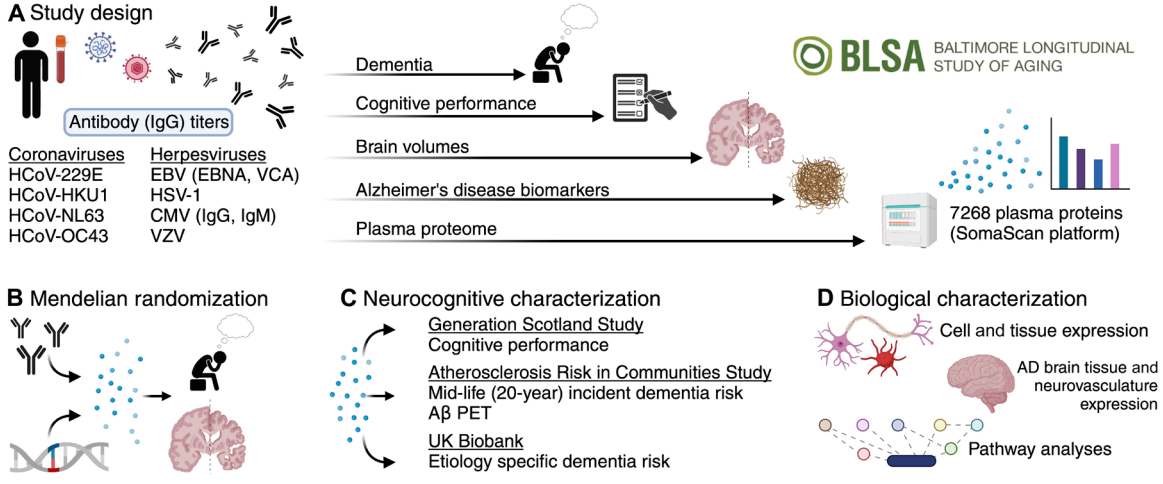

Fig. 1. Study design. (**A**) Titers of coronavirus and herpesvirus antibodies were measured in BLSA participants. Viral titers were associated with prevalent dementia, cognitive performance across five domains, regional brain volumes, ADRD plasma and PET biomarkers, and the plasma proteome (SomaScan; 7268 proteins). (**B**) Two-sample MR examined evidence for a causal link of viral titer–related plasma proteins with dementia risk and clinically relevant brain atrophy. (**C**) Candidate plasma proteins were associated with cognitive performance in the Generation Scotland (GenS) study, 20-incident dementia risk and odds of Aβ+ PET status in the Atherosclerosis Risk in Communities (ARIC) study, as well as etiology specific dementia risk in the UK Biobank (UKB). (**D**) The biological implications and functional relevance of candidate plasma proteins were assessed using multiple complementary analytic tools and open-source databases. Created in BioRender. Duggan, M. (2025) https://BioRender.com/hxnxsb2.

indices of corona and herpetic viral titers exhibited minimal correlation ($r = 0.06$, $P = 0.29$), suggesting that antibody responses were specific to different families of viruses.

Using logistic regression models adjusted for demographic, physiological, and comorbid variables, as well as sample storage time (by default controlling for seasonal/annual viral variation), we first conducted extreme group analyses by examining the associations of viral antibody titers with cognitive status among dementia cases ($n = 91$) and cognitively normal, Aβ-negative (Aβ−) PET participants ($n = 98$). We found that the odds of dementia were 51% lower with a 1 SD higher HCoV-OC43 or CMV (IgM) antibody level (Fig. 2, A and B, and table S3). In addition to cumulative burden of total antibody titers, higher tertiles of HCoV-HKU1 and CMV (IgG and IgM) antibodies were also linked to lower dementia odds (Fig. 2C and table S3). The associations of higher antibodies with lower odds of dementia were replicated for HCoV-OC43 and extended to HCoV-NL63 tertiles in analyses that included all 323 participants (rather than extreme groups; table S4). Among these participants, HCoV-OC43 antibodies were related to higher performance across all five of the examined cognitive domains, CMV (IgM) antibodies were associated with higher executive functioning and verbal fluency, and cumulative burden of total antibody titers was associated with higher executive functioning, verbal fluency, and memory (Fig. 2D and table S5). After excluding participants with dementia, higher verbal memory scores associated with cumulative burden of total antibody titers and higher verbal fluency scores associated with CMV (IgM) antibodies persisted, and associations of higher verbal fluency scores with CMV (IgG) levels emerged (table S6). HCoV-OC43 antibody's relationships with dementia, executive functioning, and verbal fluency survived false discovery rate (FDR) correction, and titer associations were not modified by self-reported sex. To assess the specificity of our results, we conducted secondary assays to measure IgG antibodies for another virus (measles) and bacteria (*Toxoplasma gondii*), but neither of these titers were related to dementia odds or cognition (tables S3 to S6).

We then determined whether coronavirus and herpesvirus antibody titers were associated with differences in 3-T magnetic resonance imaging (MRI)–derived brain volumes among BLSA participants with available neuroimaging data ($n = 223$; table S1). HCoV-NL63 antibodies were associated with greater total brain and gray matter volumes, particularly parietal and occipital gray matter (Fig. 2E and table S7). HCoV-OC43 and HCoV-229E titers were related to higher white matter volumes, especially in the frontal lobe, and VZV titers were also related to higher white matter volumes, especially in the frontal and parietal lobes. HSV-1 antibodies showed a positive association with occipital gray and white matter volumes, and CMV (IgG) antibodies showed a positive relationship with parietal gray matter. In addition, cumulative burden of coronavirus titers was related to higher total brain volume, cumulative burden of herpesvirus titers was related to higher parietal lobe volume (particularly gray matter), and cumulative burden of total viral antibody titers was related to higher total brain and gray matter volume (particularly in the parietal lobe). In contrast to the protective associations with other antibody titers, EBV (VCA) antibodies were related to lower frontal lobe volume. The associations of HCoV-NL63 titers (total brain and occipital lobe volumes) and HSV-1 tiers (occipital lobe volume) survived FDR correction, and antibody associations were not modified by self-reported sex (table S7). Together, these results suggest that participants with a more robust immune response to common corona and herpetic viruses also exhibit lower odds of dementia, higher cognitive performance, and preserved regional brain volumes.

Viral antibody titers are associated with PET and plasma ADRD biomarkers

Next, we investigated the associations of viral antibodies with odds of amyloid PET positivity in the BLSA, specifically between 73 amyloid-positive (Aβ+) and 99 Aβ− participants (table S1). A 1 SD higher HCoV-OC43 antibody was associated with 34% lower odds of Aβ+, and a 1 SD higher CMV (IgM) antibody was associated with 54% lower odds of Aβ+ (Fig. 3A and table S8). However, in analyses restricted to Aβ+ individuals, a 1 SD higher CMV (IgG) titer was associated with a 1.9-year younger amyloid onset age and 0.04 distribution volume ratio (DVR) (or 8.6 centiloids) higher mean cortical Aβ (Fig. 3, B and C, and table S8). Among participants with tau PET ($n = 36$), several coronavirus antibodies were related to greater tau deposition, including HCoV-NL63 (Braak V-VI), HCoV-229E [inferior temporal gyrus (ITG)], and HCoV-HKU1 (Braak III-IV and ITG), while cumulative burden of corona and total antibody titers were also related greater tau levels (ITG, Braak III-IV, and Braak V-VI; Fig. 3D and table S9).

Using BLSA data, we then examined the associations of coronavirus and herpesvirus antibodies with plasma ADRD biomarkers [$A\beta_{42/40}$, glial fibrillary acidic protein (GFAP), and NfL, $n = 258$; pTau-181 and pTau-231, $n = 202$; table S1]. Higher EBV (EBNA) titers were associated with lower $A\beta_{42/40}$ (reflecting higher cortical amyloid; Fig. 3E), and higher tertiles of CMV (IgM) and HSV-1 titers were also associated with lower $A\beta_{42/40}$ (Fig. 3F and table S10). Conversely, higher tertiles of HCoV-OC43, HCoV-HKU1, and EBV (EBNA) antibodies were related to lower pTau-181 (reflecting lower amyloid-induced tauopathy; Fig. 3G). No clear associations with plasma GFAP, NfL, or pTau-231 were observed. The association of cumulative coronavirus antibody burden with tau levels in the ITG survived FDR correction, titer associations were not modified by self-reported sex, and examination of secondary measles and *T. gondii* assays did not reveal relationships with ADRD biomarkers (tables S8 to S10). These findings demonstrate that participants with a more robust immune response to HCoV-OC43 consistently show better neurocognitive outcomes and suggest that several antibody titers display pleiotropic relationships with ADRD biomarkers.

Proteomic signatures of viral antibody titers

Having established the neurocognitive profiles associated with coronavirus and herpesvirus titers, we then examined the plasma proteomic signatures of these viral antibodies (7268 plasma proteins; $n = 323$; tables S1 and S11). CMV (IgM) antibodies had the strongest proteomic profile (722 proteins, $P < 0.05$; 169 proteins, FDR < 0.05), whereas HCoV-HKU1 antibodies displayed the weakest (298 proteins, $P < 0.05$; 0 proteins, FDR < 0.05), and hierarchical clustering indicated that corona- and herpetic-antibody proteomic signatures were largely distinct (Fig. 4A and table S12). None of the 220 proteins that survived FDR correction were associated with more than one viral titer. Of these proteins, 13 (6%) and 43 (20%) were differentially expressed in acute viral infection models (e.g., influenza) using SomaScan v1 and v4 platforms, respectively, suggesting that the patterns of protein expression reported here likely reflect host immune traits or prior viral exposures rather than active or unresolved viral infections (table S13). Several canonical pathways were consistently enriched in the broader proteomic profiles ($P < 0.05$) of

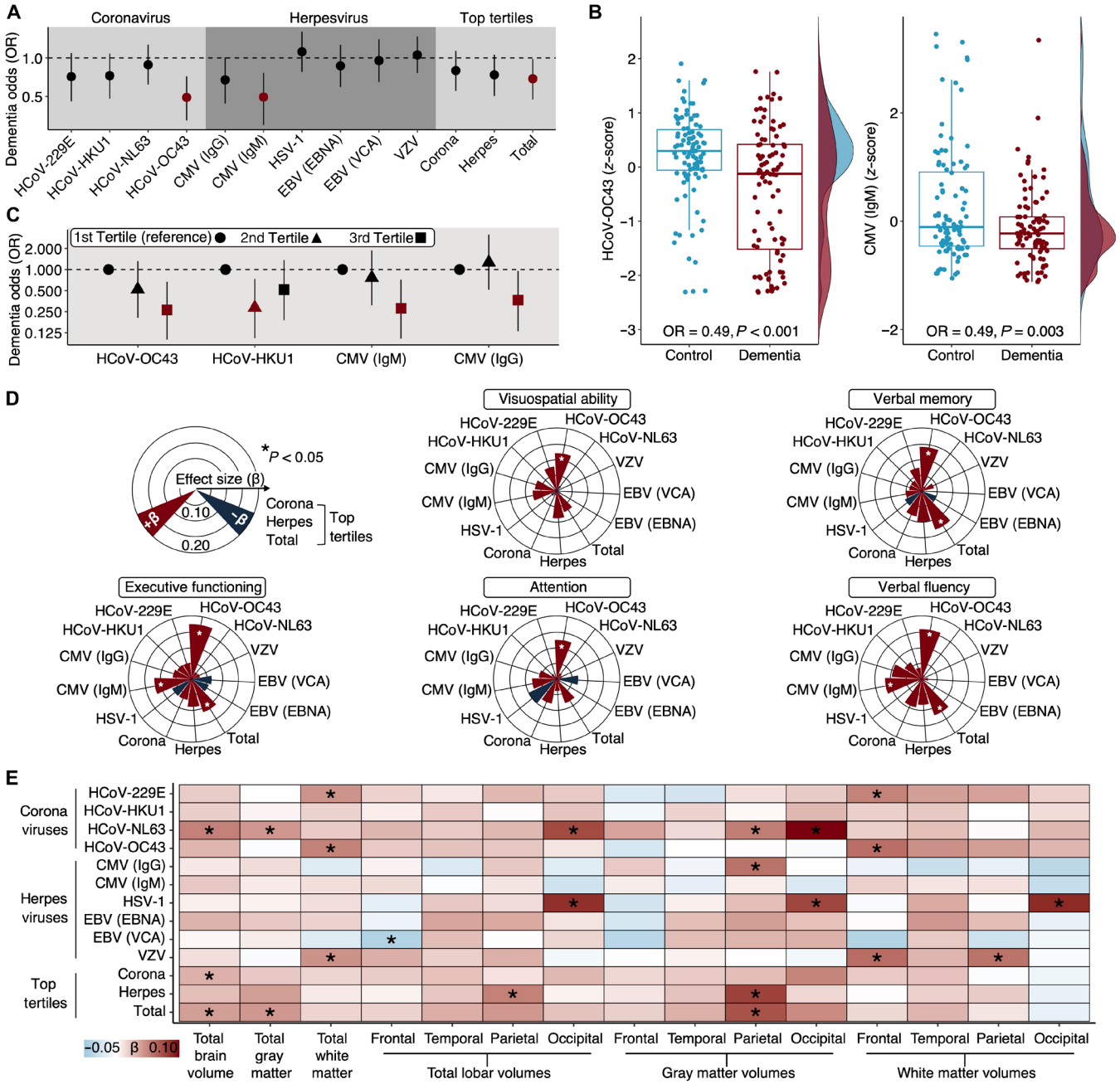

Fig. 2. Antibody titer associations with dementia, cognitive performance, and brain volumes in BLSA. (**A**) Forest plot shows the associations of viral antibody titers with odds of dementia between control (cognitively normal, Aβ−; $n = 98$) and dementia ($n = 91$) participants. Cumulative burden indices reflected the percentage of coronavirus, herpesvirus, and total (coronavirus and herpesvirus) titer measurements in the top tertile. Red shapes indicate $P < 0.05$. Results were derived from logistic regression models adjusting for age, sex, race, education, *APOEε4*, sample storage time, and a comorbidity index. OR, odds ratio. (**B**) Box plots (and corresponding density plots along *y* axes) show the distributions of HCoV-OC43 and CMV (IgM) titers between control and dementia participants. Results were derived from logistic regression models adjusting for the aforementioned covariates. (**C**) Forest plot shows antibody titer tertiles associated with odds of dementia between control and dementia participants. Results were derived from logistic regression models adjusting for the aforementioned covariates. Red shapes indicate $P < 0.05$. (**D**) Rose plots show the relationships of antibody titers with performance across five cognitive domains among all participants ($n = 323$). Results were derived from linear regression models adjusting for the aforementioned covariates. (**E**) A heatmap shows differences in regional brain volumes associated with antibody titers among participants with available 3-T MRI ($n = 223$). Results were derived from linear regression models adjusting for the aforementioned covariates plus intracranial volume. *$P < 0.05$.

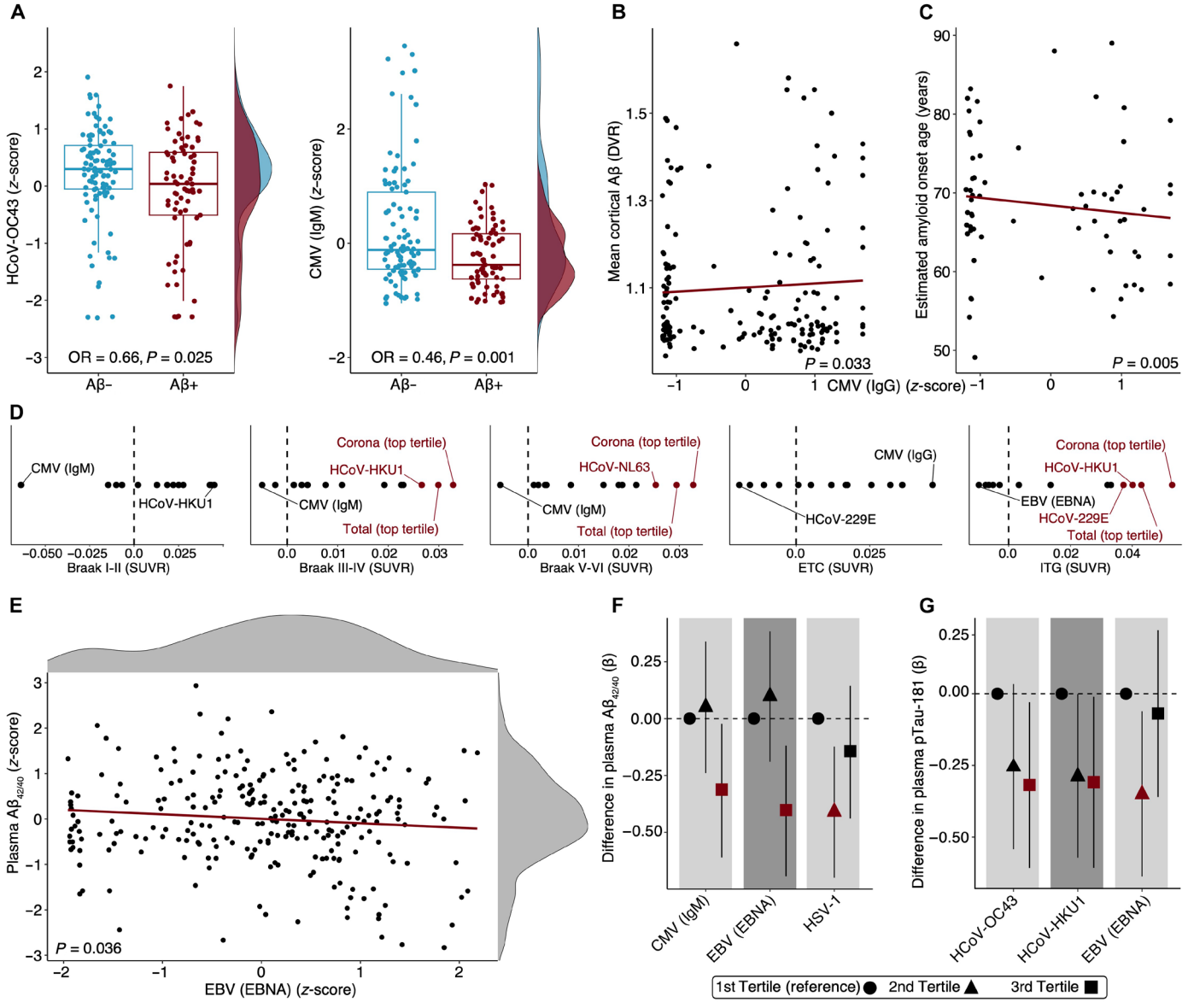

Fig. 3. Antibody titer associations with ADRD biomarkers in BLSA. (**A**) Box plots (and corresponding density plots along *y* axes) show the distributions of HCoV-OC43 and CMV (IgM) titers between Aβ− ($n = 99$) and Aβ+ ($n = 73$) PET participants. Results were derived from logistic regression models adjusting for age, sex, race, education, *APOEε4*, sample storage time, and a comorbidity index. Among Aβ+ participants, scatterplots show the associations of CMV (IgG) with (**B**) mean cortical Aβ levels and (**C**) estimated age of Aβ+ onset. Results were derived from linear regression models adjusting for the aforementioned covariates. (**D**) Jitter plots show associations of antibody titers with regional tau PET levels ($n = 36$). Results were derived from linear regression models adjusting for age, sex, amyloid PET status, and a comorbidity index. Titers that showed the strongest and weakest associations with tau levels are labeled, with red color indicating $P < 0.05$. (**E**) Scatterplot shows the association of EBV (EBNA) with plasma $A\beta_{42/40}$ ($n = 258$). Results were derived from linear regression models adjusting for age, sex, race, education, *APOEε4*, sample storage time, estimated glomerular filtration rate (eGFR), and a comorbidity index. Forest plots show antibody titer tertiles associated with (**F**) plasma $A\beta_{42/40}$ ($n = 258$) and (**G**) plasma pTau-181 ($n = 202$). Results were derived from linear regression models adjusting for the aforementioned covariates. Red shapes indicate $P < 0.05$.

viral titers, including (i) immunological processes (e.g., interleukin signaling), (ii) cellular mechanisms implicated in neurodegenerative diseases (e.g., proteostasis), (iii) gene regulatory processes (e.g., translation termination), (iv) blood-brain barrier components (e.g., neurovascular coupling), and (v) viral response pathways (e.g., coronavirus pathogenesis; Fig. 4B, figs. S5 to S7, and table S14). Viral antibody proteomic signatures were also enriched for immune- and brain tissue–specific proteins, as well as proteins preferentially expressed by adaptive (e.g., B and T cells) and innate (e.g., macrophages, neutrophils, and mast cells) immune cells (tables S15 and S16). Twelve plasma proteins were differentially expressed across five or more antibody titers at an uncorrected threshold ($P < 0.05$; Fig. 4C), henceforth referred to as candidate proteins.

The directions of candidate protein associations were generally consistent; for example, IGDCC4 was positively associated with CMV (IgM), EBV (EBNA), HCoV-NL63, HCoV-HKU1, and HCoV-229E, and these relationships did not vary by *APOEε4* genotype (table S17). However, several candidate proteins (i.e., LAG3, TBX5, DDIT4, PRSS27, and

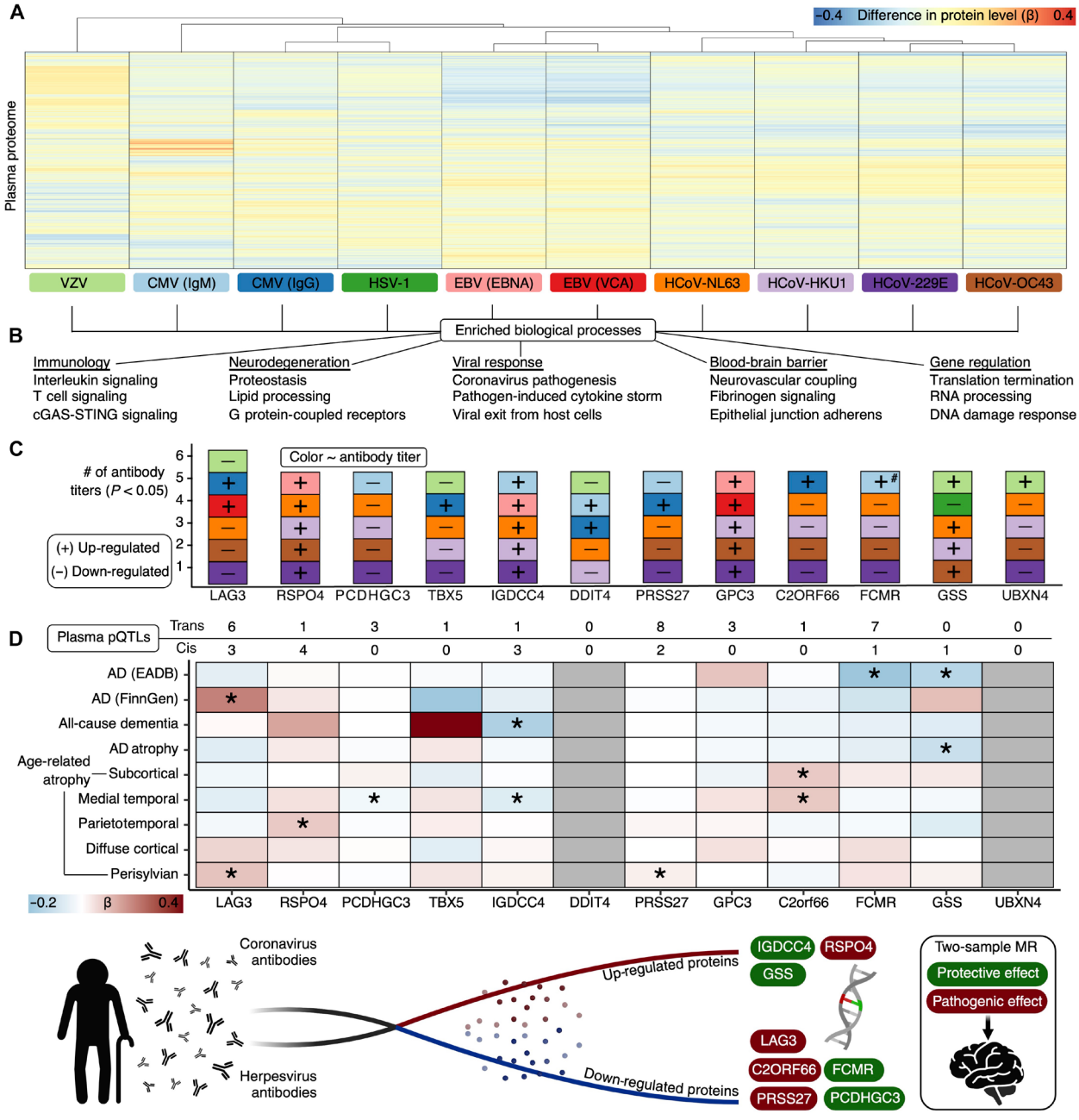

Fig. 4. Antibody titer associations with the plasma proteome in BLSA and two-sample MR. (**A**) Heatmap shows differences in the plasma proteome (SomaScan; 7268 proteins) associated with antibody titers ($n = 323$). Dendrogram reflects hierarchical clustering using Euclidean distances. Results were derived from linear regression models adjusting for age, sex, race, education, *APOEε4*, sample storage time, eGFR, and a comorbidity index. (**B**) Summary of enriched biological processes in the plasma proteomic signatures ($P < 0.05$) of antibody titers. Results were derived from ingenuity pathway analysis. cGAS-STING, cyclic GMP-AMP synthase - stimulator of interferon genes. (**C**) A clustered bar graph shows plasma proteins associated with five or more antibody titers ($P < 0.05$). (+) and (−) indicate higher or lower protein levels were associated with a given titer. # indicates an association that survived FDR correction. (**D**) A modified heatmap shows the results of two-sample MR analyses that assessed the relationships of genetically determined plasma protein levels with genetic susceptibility for neurocognitive outcomes, along with a corresponding graphic summarizing these findings. Protein quantitative trait loci (pQTLs) were obtained from deCODE Genetics. AD GWAS was obtained from European Alzheimer & Dementia Biobank (EADB) and FinnGen, all-cause dementia (ACD) GWAS was obtained from FinnGen, and neuroimaging signature GWAS was obtained from the UKB. *$P < 0.05$. Created in BioRender. Duggan, M. (2025) https://BioRender.com/u8a6ebo.

C2ORF66) showed divergent associations with CMV (IgG). We suspected that these 12 candidate proteins may be especially important molecular mediators of host immune responses due to their associations with multiple viral antibodies, and we subsequently examined their potential causal contributions to neurocognitive outcomes.

Genetic variation underlying candidate proteins is causally linked to neurocognitive outcomes

To gain mechanistic insights and identify potential causal relationships, we determined whether genetic variation that predicts candidate protein abundance in plasma may influence AD and all-cause dementia (ACD) risk, as well as machine learning–derived measures of distinct aging and AD-related brain atrophy patterns. Specifically, we conducted two-sample MR after combining candidate plasma protein quantitative trait loci (pQTLs) identified by the deCODE study ($n = 35{,}559$) with GWAS summary statistics of AD from the European Alzheimer & Dementia Biobank (EADB; $n = 487{,}511$; cases = 39,106), AD ($n = 214{,}893$; cases = 3899) and ACD ($n = 211{,}397$; cases = 7395) from the FinnGen project, and six validated neuroimaging signatures from the UK Biobank (UKB) ($n = 33{,}541$; AD-atrophy patterns, age-related atrophy patterns in subcortical, medial-temporal, parietotemporal, diffuse cortical, and perisylvian regions) (*21*–*25*). Ten candidate proteins maintained at least one pQTL instrumental variable (table S18).

We found evidence supporting neuroprotective effects of two candidate proteins that were up-regulated with viral antibodies (IGDCC4 and GSS) and neuropathogenic effects of three candidate proteins that were down-regulated with viral antibodies (PRSS27, C2ORF66, and LAG3; Fig. 4D and tables S19 and S20). For example, IGDCC4 was consistently up-regulated with viral titers and MR analyses using three cis-pQTLs and one trans-pQTL causally implicated this protein in dementia risk reduction (ACD) and the maintenance of medial temporal brain volume with increasing age. Sensitivity analyses using the weighted median method confirmed these findings, while MR Pleiotropy Residual Sum and Outlier (MR-PRESSO) analyses additionally supported IGDCC4's causal relationships with preserved medial temporal brain volumes. However, several proteins did not show this trend (FCMR, PCDHGC3, and RSPO4). Leveraging SomaScan plasma and cerebrospinal fluid (CSF) protein measurements from the Johns Hopkins CSF Cohort ($n = 194$), we found that only LAG3 and FCMR were correlated across biofluids, indicating that the potential causal roles of candidate proteins in neurodegeneration may be primarily attributed to their effects in peripheral circulation (table S21). Along with demonstrating that several candidate proteins play a mechanistic role in neurodegeneration, these findings also indicate that beneficial viral antibody associations identified in preceding BLSA analyses may be attributed to an up-regulation of neuroprotective proteins and a down-regulation of neuropathogenic proteins (Fig. 4D).

IGDCC4 is a key mediator of neurodegeneration

Given that IGDCC4 was the only candidate protein which showed (i) causal associations with both clinical and neuroimaging outcomes, (ii) a consistent pattern of regulation across viral antibody titers, and (iii) primarily cis-plasma pQTLs (i.e., supporting a gene-protein outcome relationship), this unique protein was selected for additional follow-up analyses. Leveraging computed results from the Generation Scotland (GenS) cohort (*26*) ($n = 1065$), we found that plasma IGDCC4 was related to higher performance in nonverbal reasoning, verbal fluency, vocabulary, processing speed, and general cognition (Fig. 5A and table S22). We also used data from the Atherosclerosis Risk in Communities (ARIC) study, where a blood draw in mid-life (visit 2; $n = 11{,}596$) was followed by 20-year dementia surveillance through late life (visit 5) when Aβ PET scans were acquired for a subset of participants ($n = 260$). Here, each $\log_2$ increase in plasma IGDCC4 abundance in mid-life was associated with 79% lower odds of Aβ+ 20 years later, as well as a 33% decreased risk of ACD over this same follow-up period; furthermore, the same increase in plasma IGDCC4 abundance in late life was similarly associated with 70% lower odds of Aβ+ ($n = 272$; Fig. 5B and tables S23 and S24). To examine IGDCC4's relationships with etiology-specific dementia risk, we used Olink proteomic data from the UKB ($n = 41{,}344$), where we found that plasma IGDCC4 abundance was not significantly related to ACD or other dementia subtypes over a 14-year follow-up period, but showed trending opposite associations with AD [hazard ratio (HR) = 1.28; 95% confidence interval (CI), 0.94 to 1.74; $P = 0.117$] and vascular dementias (VaDs; HR = 0.69; 95% CI, 0.42 to 1.13; $P = 0.139$; Fig. 5C and tables S25 and S26). This inverse association between plasma IGDCC4 and VaD was reported previously in a genetic inference study, although this relationship did not survive correction for multiple comparisons (*27*). While the lack of UKB statistical significance may be due to variability in IGDCC4's measurements across platforms (SomaScan and Olink; $r = 0.66$), IGDCC4's opposite patterns with AD and VaD could also suggest that its associations with dementia risk are contingent on cerebrovascular pathology (i.e., ARIC has 4.6-, 2.3-, and 2.1-fold higher prevalence of diabetes, hypertension, and smoking, respectively, compared to UKB; tables S23 and S25).

Considering its consistent protective associations with neurocognitive outcomes across multiple independent cohorts, we then examined whether genetic variation that influences IGDCC4 protein levels in CSF may be mechanistically relevant to clinical and neuroimaging outcomes. Because of their causal associations with plasma IGDCC4 identified in preceding two-sample MR analyses, we combined GWAS summary statistics of ACD from the FinnGen project and age-related medial temporal atrophy from the UKB with four cis- and one trans-CSF pQTLs identified by Washington University (WashU; $n = 3107$) and conducted two-sample MR (*22*–*24*, *28*). Consistent with prior results, we found evidence supporting a causal relationship of CSF IGDCC4 abundance with dementia risk reduction (ACD) and the maintenance of medial temporal brain volume with increasing age (Fig. 5D and tables S27 to S29). Sensitivity analyses using the weighted median method confirmed these findings, while MR-PRESSO analyses additionally supported IGDCC4's causal relationship with dementia risk reduction. Because IGDCC4 displayed limited correlation across biofluids (plasma/CSF) in preceding analyses and IGDCC4's MR analyses across these same biofluids relied on largely distinct genetic instruments [i.e., CSF and plasma pQTLs shared one common trans–single-nucleotide polymorphism (SNP) but were otherwise unique cis-SNPs], these patterns could suggest that IGDCC4's causal contributions to neurodegeneration in peripheral and central circulation are temporally discrete. Together, these results indicate that intrathecal abundance of IGDCC4 is mechanistically relevant to neurodegeneration and may play a particularly important role in mediating protective effects on neurocognitive outcomes.

Biological characterization of IGDCC4

Existing studies have externally validated the IGDCC4 SomaScan protein measurement (table S30). Previously published results with

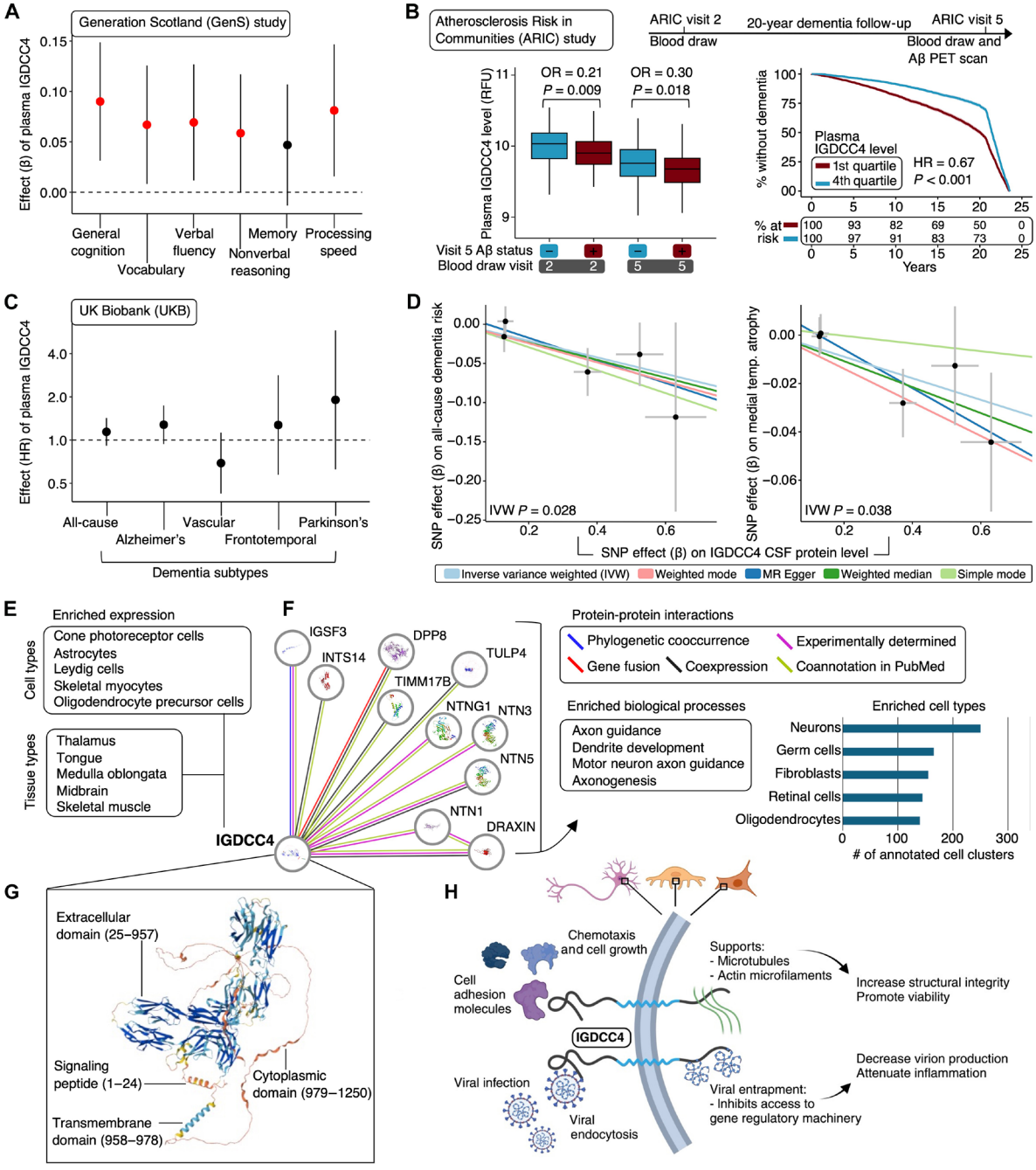

Fig. 5. IGDCC4 associations with neurocognitive outcomes in external cohorts and biological characterization. (**A**) Forest plot shows plasma IGDCC4 associations with cognitive performance in the GenS cohort ($n = 1065$). Results were derived from linear mixed-effects regression models adjusting for kinship matrix, age, sex, depression diagnosis, clinic study site, and sample storage time. Orange color indicates $P < 0.05$. (**B**) Box plots show IGDCC4 distributions measured at visit 2 ($n = 260$) and visit 5 ($n = 272$) across participants with differing Aβ PET status at visit 5 in the ARIC study. A Kaplan-Meier plot shows the observed 20-year dementia event-free probabilities grouped according to upper/lower IGDCC4 quartiles ($n = 11,596$). HR reflects the association with continuous protein measurements. Results were derived from logistic or Cox regression models adjusting for age, sex, race-center, education, *APOEε4*, eGFR, and cardiovascular risk factors. (**C**) Forest plot shows the associations of IGDCC4 with 14-year risk of dementia in the UKB ($n = 41,344$). Results were derived from Cox regression models adjusting for age, sex, study site, education, *APOEε4*, eGFR, and cardiovascular risk factors. (**D**) Scatterplots show two-sample MR results that assessed the relationships of genetically determined IGDCC4 protein levels in CSF with genetic susceptibility for ACD and age-related medial temporal atrophy. pQTLs were obtained from WashU. ACD GWAS was obtained from FinnGen, and neuroimaging signature GWAS was obtained from the UKB. (**E**) Top-five cell and tissue types with the highest IGDCC4 expression. Transcriptomics data were sourced from the Human Protein Atlas. (**F**) IGDCC4 protein-protein interaction (PPI) network and corresponding enriched biological process and cell types for this network. Results were derived from the STRING and PanglaoDB. (**G**) Predicted conformation of IGDCC4; domains are labeled with corresponding amino acid sequences. Image sourced from AlphaFold. (**H**) Working model of IGDCC4's potential cellular mechanisms underlying its relationships with viral infections and neurocognitive outcomes. Created in BioRender. Duggan, M. (2025) https://BioRender.com/4hiujxt.

electronic health records from the UKB (n = 46,218; Olink) and deCODE (n = 35,892; SomaScan) (*29*) showed that higher plasma IGDCC4 abundance was related to lower odds of multiple (especially respiratory) infection diagnoses, while data from WashU and the Massachusetts General Hospital (both SomaScan) showed higher plasma IGDCC4 was related to lower odds of SARS-CoV-2 hospitalization and ventilation (*30*) (table S31). Using a subset of UKB participants with available data (n = 817), we found that plasma IGDCC4 abundance (Olink) was related to lower antigen-specific antibody levels of EBV (early diffuse antigen) and CMV (pp28 antigen), with data from the Religious Orders Study/Rush Memory and Aging Project (ROSMAP; n = 270) also showing that plasma IGDCC4 abundance (SomaScan) was related to lower CMV (IgG) titers (tables S32 and S33). Given IGDCC4's consistent positive relationships with coronavirus and herpesvirus titers in the BLSA (i.e., a cohort where higher antibody titers were related to better neurocognitive outcomes), these negative relationships observed in external cohorts could suggest that a more robust immune response to viruses is accompanied by an up-regulation of circulating IGDCC4 levels that is otherwise attenuated among individuals who are susceptible to infections and neurodegeneration.

In addition to immune cell–specific expression patterns (e.g., monocytes), publicly available single-cell and bulk-tissue transcriptomics data showed enriched expression of IGDCC4 in several CNS cell types (e.g., astrocytes) and brain regions (e.g., thalamus) (Fig. 5E, fig. S8, and table S34). Single-cell RNA sequencing (RNA-seq) of brain parenchyma cell types showed that IGDCC4 was down-regulated in inhibitory neurons among individuals with early AD pathology and in excitatory neurons among individuals with any AD pathology (fig. S8 and table S35). Single-cell RNA-seq of neurovascular cell types also showed that IGDCC4 was primarily down-regulated in AD (i.e., up-regulated in oligodendrocytes and perivascular/meningeal fibroblasts but down-regulated in capillary endothelial cells, oligodendrocyte precursor cells, T cells, and solute-transport pericytes; fig. S8 and table S36). In addition to clinical AD tissue, IGDCC4 was down-regulated at the protein level (i.e., via mass spectrometry) in the hippocampus of 5xFAD mice and down-regulated at the RNA level (i.e., via bulk transcriptomics) in the hippocampus of APP/PS1 mice (table S37). Together, these results suggest that IGDCC4 is (i) enriched in brain tissue and CNS cell types, (ii) down-regulated in neurons and neurovascular cell types in AD brains, and (iii) down-regulated in clinically relevant brain regions in AD mouse models.

Protein interaction analyses revealed IGDCC4's extensive network with regulators of axonal integrity, including ample coexpression patterns and experimentally verified interactions with the netrin family of cell adhesion proteins (Fig. 5F and table S38). This network was enriched for axonal guidance and axonogenesis and for expression in several CNS cell types (e.g., neurons; tables S39 and S40). IGDCC4's canonical functions are largely uncharacterized, but similar to other immunoglobulin superfamily members with dual cell adhesion and immunological roles, its associations in the current study may be attributed to its unique functional domains that facilitate cross-talk between cellular growth, structural integrity, and defense response mechanisms (Fig. 5G). As a transmembrane glycoprotein, IGDCC4's extracellular domain can bind to cell adhesion molecules [resulting in cell growth and stabilization of cytoskeletal components by its cytoplasmic domain (*31*)] and facilitate viral internalization [triggering viral entrapment by its cytoplasmic domain (*32*); Fig. 5H]. Therefore, the protective effects on neurocognitive outcomes associated with higher circulating IGDCC4 abundance may reflect this protein's basic capacity to enhance cellular structural integrity (hence its associations with axonal viability) and arrest virion production in the context of viral exposure.

DISCUSSION

The current multiomic investigation characterized the neurocognitive and plasma proteomic profiles of four coronavirus and six herpesvirus antibody titers in a community-based cohort of older adults. Participants who maintained a more robust immune response to several viruses (especially HCoV-OC43) showed better neurocognitive outcomes (i.e., lower odds of dementia, higher cognitive performance, and regional brain volumes), mixed relationships with some ADRD biomarkers, and plasma proteomic signatures enriched with immunological and neurologically relevant biological processes. Using genetic inference techniques, we found that the associations between circulating antibody titers, dementia, and dementia endophenotypes may be attributed to altered expression of mechanistically relevant proteins in plasma. One of these proteins, IGDCC4, was related to 20-year incident dementia risk, cognitive functioning, and Aβ+ risk using data from two independent cohorts, while its plasma and intrathecal abundance were causally linked to dementia risk and clinically relevant brain atrophy. Together, our findings reveal the neurocognitive and plasma proteomic signatures of viral antibodies and implicate IGDCC4 as an important molecular mediator of neurodegeneration.

Prior investigations have reported the protective effects associated with herpetic titers observed in our study (*7*–*11*), while other studies have reported deleterious or null effects of herpes viruses (*33*, *34*). We add to existing literature by showing that these protective effects may extend to antibody titers of common coronaviruses. Despite minimal correlation between cumulative burden indices for these two groups of antibodies, several coronavirus and herpesvirus titers were related to higher cognitive functioning and preserved brain volumes, suggesting that greater capacities to mount generalized immune responses against common viruses (due to host genetic factors and/or differences in exposures) may render some individuals more resilient to neurodegeneration. This postulation is supported by studies showing that (i) the activation of innate and adaptive antiviral defense mechanisms in the periphery (e.g., boosting Toll-like receptor 9 signaling, increasing populations of antibody-producing B cells, etc.) can attenuate neuropathology and cognitive decline by triggering homeostatic microglial functions (*35*, *36*), (ii) genetic variation in host immune traits can influence vulnerability to infection and neurodegeneration (*37*, *38*), and (iii) mild, systemic pathogenic exposures can elicit protective neuroimmune mechanisms that mitigate brain amyloidosis (*39*). The lack of associations with measles and *T. gondii* titers in secondary analyses suggests that the observed relationships with neurocognitive outcomes may be specific to viruses circulating in the community, rather than bacteria or more rare viral agents. While the discordant associations of some antibody titers (particularly CMV and EBV) with ADRD biomarkers could reflect the pleiotropic or disease stage–dependent relationships between immune functioning and AD neuropathology (*40*–*42*), they may also reflect variable contributions of Aβ's antiviral properties (*43*). The consistent effects associated with HCoV-OC43 antibodies (i.e., lower pTau-181, lower odds of dementia and Aβ+, higher white matter volumes, and cognitive performance across all domains) may be attributed to this virus's unique neurotropism (*44*), its capacity to induce adaptive immune responses that protect against more severe

infections (*45*, *46*), or its higher prevalence relative to other viruses examined in our study (*47*, *48*). Along with differences in neurotropism, host immune responses, and prevalence, the broader differential associations of some coronavirus titers but not others may be attributed to their unique virology (e.g., distinct viral life cycles, cell-specific tropism, etc.) or other biological factors (e.g., faster clearance of some viral proteins).

Our findings establish how viral antibodies relate to the peripheral proteome beyond select inflammatory markers measured in single-plex assays and extend our understanding of the biological mechanisms by which host immune predispositions to viruses may influence neurodegeneration. Given that 94.7% of participants did not show evidence of an active infection, as well as the limited overlap with acute viral infection models, we suspect that the patterns of protein expression reported here may reflect host immune traits or prior viral exposures that render some individuals resistant to infection or maladaptive inflammatory responses. We also suspect that these patterns of protein regulation accurately reflect differences in circulating antibody titers because their proteomic profiles were enriched with immune tissue- and cell-specific proteins, as well as canonical immune and viral response pathways. Although the direction of candidate protein expression with respect to different viral antibodies was generally consistent, the divergent relationships of some proteins with CMV and EBV antibodies may be related these viral titers' discordant associations with ADRD biomarkers. Using genetic techniques to infer causality, we found that the neurocognitive profiles associated with antibody titers may be attributed to an up-regulation of candidate proteins that exert beneficial mechanistic effects and a down-regulation of candidate proteins that exert deleterious mechanistic effects, consistent with other studies showing that changes in the plasma proteome triggered by immune insults or host immune factors can influence dementia risk and neurodegeneration (*6*, *16*, *49*). Given that candidate proteins exhibited limited correlations across plasma and CSF, their potential causal roles in neurodegeneration may be primarily attributed to their effects in peripheral circulation, similar to other proteins that are not expressed at meaningful levels in the CNS but, nonetheless function as reliable biomarkers for, and as causal mediators of, neurodegenerative diseases (e.g., growth differentiation factor 15 and vascular cell adhesion molecule–1) (*17*, *50*).

Multicohort, orthogonal evidence implicated IGDCC4 as a sensitive predictor of neurologic health and a molecular determinant that links host immune responses to neurodegeneration. Our results add to existing studies that have demonstrated the neuroprotective roles of other immunoglobulin superfamily members, including decreased rates of Aβ deposition associated with soluble TREM2 (*40*) and preserved cognitive functioning and decreased Aβ production related to CD147 (*51*, *52*). While we hypothesize that the benefits associated with higher circulating IGDCC4 may be attributed to its basic capacity to enhance cellular structural integrity and arrest virion production in the context of viral exposure, its enriched expression in brain tissue and its causal, mechanistic roles across plasma and CSF indicate that this protein's effects may be exerted in both peripheral and CNS cell types. Along with its predominantly cis-pQTLS, IGDCC4's associations with lower antibody levels and odds of symptomatic infections in external cohorts but consistent positive associations with viral titers in the BLSA could indicate that this protein's up-regulation is an adaptive process triggered by viral exposures or host immune traits that is otherwise blunted among individuals who are susceptible to viral infections and neurodegeneration. Although there are no approved drugs targeting IGDCC4, this membrane-bound protein is highly accessible to antibody-based biologics, suggesting that it may be an attractive candidate for activating monoclonal therapies that are under development for other immunoglobulin superfamily members [e.g., TREM2 (*53*)].

The current study has several strengths, including multimodal characterization of viral serology in a deeply phenotyped cohort, state-of-the-art proteomics, genetic techniques to support causality, and multicohort replication. However, this study also has several limitations. First, our results may have been influenced by residual confounding from unmeasured variables jointly associated with viral exposures and neurocognitive outcomes. Second, although no participants maintained an active diagnosis of an infection examined in the current study, unresolved or emerging viral infections may have been present at the time of blood draw, which were not otherwise manifested in symptomatology. Additional investigations should use longitudinal serology to establish the stability of asymptomatic viral titers over time and determine whether individual-specific rates of change in antibody levels may modulate effects on neurocognitive outcomes. Third, because of this study's exploratory nature and the modest number of participants, we had limited power to detect significant effects at an FDR-corrected threshold and therefore did not adjust *P* values for multiple comparisons in primary analyses. Although we applied orthogonal strategies to reduce potential type 1 error and despite several candidate proteins having been previously implicated in AD [e.g., LAG3, GSS, and PCDHGC3 (*54*–*56*)], additional studies will be needed to validate our findings. Fourth, immune responses to other viruses that were not assessed in the present analyses may have influenced our study's conclusions, and idiosyncratic effects of antibody measurements (e.g., cross-reactivity) may have affected the sensitivity and specificity of titer quantifications. To capture the repertoire of viral immune responses more accurately and to deconvolute the relationships among viral exposures, infections, and neurodegeneration more reliably, future studies are encouraged to use complementary techniques to measure viral abundance [i.e., serology, polymerase chain reaction (PCR), and antigen tests]. Despite these limitations, our results reveal associations between viral antibody titers and neurocognitive outcomes in a community-based cohort of older adults, while highlighting the circulating molecular conduits that may link host immune responses to neurodegeneration.

MATERIALS AND METHODS

Baltimore Longitudinal Study of Aging

The current study used data from the BLSA, a community-based cohort that has continuously enrolled participants since 1958 (*57*). Comprehensive health and functional screening evaluations (including blood draws) were conducted at enrollment and at each study visit, which occurred biennially until 2005 and then every 1 to 4 years depending on age (age < 60 years, every 4 years; age 60 to 79 years, every 2 years; age ≥ 80 years, every year). Participants were eligible for the current analyses if they had an available blood sample, which was collected concurrently with neurocognitive outcomes examined in the current study (e.g., MRI scan) using standardized protocols and frozen at −80°C until analysis. The current study prioritized selection of BLSA participants with dementia ($n = 91$; 17 with PET scan) or a PET scan ($n = 172$); we also selected another set of BLSA participants at random ($n = 77$), for a total sample size of 323. Vaccination records were unavailable. The current manuscript follows the

Strengthening the Reporting of Observational Studies in Epidemiology reporting guidelines.

BLSA viral antibody measurements

Solid-phase chemiluminescence assays (Meso Scale Discovery) were used to measure IgG antibodies to the following HCoVs: HCoV-OC43, HCoV-HKU1, HCoV-NL63, and HCoV-229E. Solid-phase enzyme immunoassays (IBL-America) were used to measure IgG antibodies to the following human herpesviruses: CMV, HSV-1, VZV, EBV-EBNA, EBV-VCA, and IgM antibodies to CMV. To assess the specificity of coronavirus and herpesvirus titer results, in secondary analyses we also measured IgG antibodies to measles and *T. gondii* using similar solid-phase enzyme immunoassays. Assay procedures and parameters have been described previously (*20*, *58*, *59*). Standardized continuous titer measurements, their tertiles, and cumulative burden indices [i.e., percentage of measurements in the top tertiles of coronavirus, herpesvirus, and total (coronavirus and herpesvirus)] were examined as predictors. Serostatus was not assessed, as older adults have high rates of seropositivity and meaningful cut points among these individuals can be unreliable (*20*).

BLSA cognitive status

Cognitive status was adjudicated by an expert panel of physicians and specialists, as detailed previously (*60*). Briefly, participant serial clinical and neuropsychological data were reviewed at each consensus case conference if the participant had >3 errors on the Blessed Information-Memory-Concentration test or ≥0.5 total combined score on the Clinical Dementia Rating Scale. Mild cognitive impairment was based on Petersen's criteria. Dementia was based on the criteria outlined in the *Diagnostic and Statistical Manual of Mental Disorders*, Third Edition, and the National Institute of Neurological and Communicative Disorders and Stroke-Alzheimer's Disease and Related Disorders Association.

BLSA cognitive performance

Composite scores of five cognitive domains—visuospatial ability, verbal memory and fluency, executive functioning, and attention—were calculated from standardized (converted to a *z*-score using the baseline mean and SD) and averaged individual task components, as described previously (*3*). As certain cognitive tasks were initiated in the BLSA at different periods according to protocol changes, composite scores for participants at each visit were computed from those tasks available at the time of assessment. Visuospatial ability was measured using a modified version of the Educational Testing Service Card Rotations Test and two Clock Drawing Tests (CDTs), where participants were asked to draw the hands and face of clocks indicating 3:25 and 11:10; a composite score was then calculated using the average of the standardized *z*-scores from the Card Rotations Test and the mean of the CDTs. Verbal memory was measured using immediate (sum of five learning trials) and long-delay free recall from the California Verbal Learning Test. Verbal fluency was measured using verbal fluency—letters (F, A, and S) and verbal fluency—categories (fruits, animals, and vegetables). Executive functioning was measured using Trail Making Test Part B and the Digit Span Backward subset of the Wechsler Adult Intelligence Scale—Revised. Attention was measured using Trail Making Test Part A and the Digit Span Forward subset of the Wechsler Adult Intelligence Scale—Revised. Scores of Trail Making Test Part A and Part B were first natural log transformed, *z*-scored, and then signs inverted, so that higher scores reflect higher performance (i.e., consistent with the direction of performance of other cognitive tasks).

BLSA 3-T brain MRI

T1-weighted magnetization-prepared rapid gradient echo scans were acquired on a 3-T Philips Achieva (repetition time = 6.8 ms, echo time = 3.2 ms, flip angle = 8°, image matrix = 256 by 256, 170 slices, pixel size = 1 mm by 1 mm, slice thickness = 1.2 mm, sagittal acquisition). We applied a validated, Multi-Atlas Region Segmentation Utilizing Ensembles anatomic labeling method specifically designed to achieve a consistent parcellation of brain anatomy in longitudinal MRI studies using T1-weighted sequences (*61*). Analyses adjusted for intracranial volume (defined at age 70) and examined standardized values of total brain, gray matter, white matter, and lobar volumes (frontal, parietal, occipital, and temporal).

Baltimore Longitudinal Study of Aging positron emission tomography

^{11}C-Pittsburgh compound-B (PiB) DVRs and ^{18}F-flortaucipir standardized uptake value ratios (SUVRs) were measured using PET (*62*). Aβ scans (70 min) were acquired on a GE Advance or a Siemens high-resolution research tomograph (HRRT) scanner immediately following an intravenous bolus injection of ~555 megabecquerel (MBq) of the radiotracer. Using cerebellar gray matter as a reference, DVRs were computed with a spatially constrained simplified reference tissue model. Mean cortical Aβ reflected the average DVR values across the cingulate, frontal, parietal (including precuneus), lateral temporal, and lateral occipital regions, excluding the pre- and postcentral gyri. Mean cortical DVR values were harmonized between the two scanners by leveraging longitudinal data available on both scanners for 79 participants. Aβ status (+/−) was defined on the basis of a Gaussian mixture model threshold of 1.064 mean cortical DVR (*62*). Age of Aβ onset reflected the estimated age at which a participant became Aβ+ and was calculated using nonlinear mixed-effects models incorporating random effects, as described previously (*63*). Participants who converted from Aβ− to Aβ+ ($n = 7$) had ≥3 scans; for these participants, observations at which a participant's Aβ status reflected the participant's status at ≥50% of scans were retained. One participant who converted from Aβ+ to Aβ− across their only two scans was excluded. Tau PET scans (30 min) were acquired on a Siemens HRRT scanner 75 min after an intravenous bolus injection of ~370 MBq of the radiotracer. Using PET images partially volume corrected with the region-based voxelwise method, SUVRs were computed with the inferior cerebellar gray matter as a reference. Averaged bilateral SUVRs for five regions of interest (ROIs)—Braak composite ROIs (i.e., unique ROIs corresponding to Braak stages I-II, II-IV, and V-VI), the entorhinal cortex (ETC), and the ITG—were examined because of their relevance to cortical Aβ pathology (*64*, *65*). Braak stage–specific SUVR calculations used an established Braak staging system that approximated the anatomical definitions of transentorhinal (I-II), limbic (III-IV), and isocortical (V/VI) Braak stages (*64*, *66*).

BLSA ADRD plasma biomarkers

ADRD plasma biomarkers were measured on the single-molecule array (Simoa) HD-X instrument (Quanterix), as described previously (*3*, *62*). $A\beta_{40}$, $A\beta_{42}$, GFAP, and NfL were quantified using the Neurology 4-Plex E assay. Samples were run in duplicate, and values were averaged; coefficients of variation (CVs) were 1.5, 1.0, 4.9, and 4.8% for $A\beta_{40}$, $A\beta_{42}$, GFAP, and NfL, respectively. pTau-181 and

pTau-231 were measured using a validated in-house Simoa assay (*62*, *67*). Repeatability coefficients were 5.3% for pTau-181 (5.1% for 11.6 pg/ml and 5.5% for 15.5 pg/ml) and 5.8% for pTau-231 (3.4% for 31.6 pg/ml and 7.4% for 42.7 pg/ml). GFAP, NfL, pTau-181, and pTau-231 were $\log_2$ transformed. $A\beta_{42/40}$ ratio and standardized values were used in analyses.

BLSA plasma proteomics

The plasma proteome was assessed using the SomaScan v4.1 platform (7288 SOMAmer reagents), as described previously (*68*). Using 102 blind duplicates, aptamers with an intra-assay CV of >50% were excluded ($n = 20$), and the median intra-assay CV was 4.5%. Values were $\log_2$ transformed, and those beyond 5 SDs were winsorized. Entrez Gene IDs were used as labels for corresponding aptamers.

BLSA genetics

Genome-wide genotyping was performed using the Illumina 550K or NeuroChip platforms using standard quality control (QC) procedures described previously (*6*). Variants were excluded for poor call rate (missing > 1%), violations of Hardy-Weinberg equilibrium ($P < 1 \times 10^{-6}$), and limited minor allele frequency (<1%). Samples were excluded for poor genotyping efficiency (missing > 2%), sex inconsistencies (i.e., discordance between chromosomal and self-reported sex), cryptic relatedness (pihat > 0.25), or if they were not of European ancestry by self-report or principal component detection. Imputation was performed for Illumina 550K or NeuroChip datasets separately with the Michigan Imputation Server MaCH (https://imputationserver.sph.umich.edu/) using the HRC r1.1.2016 reference panel. After imputation, datasets were merged, overlapping samples were removed, and SNPs with low imputation quality ($R^2 < 0.9$), minor allele frequencies < 1%, Hardy-Weinberg equilibrium $P < 1 \times 10^{-6}$, and those that did not overlap between the two datasets (missingness < 99%) were excluded. The final genetic dataset included 5,439,477 SNPs.

BLSA covariates

Baseline age (years), sex (male/female), race (white/non-white), and education level (years) were defined on the basis of self-report. *APOEε4* carrier status (0 ε4 alleles/≥1 ε4 alleles/missing) was defined via PCR with restriction isotyping using the type IIP enzyme Hha I or the TaqMan method. Estimated glomerular filtration rate (eGFR)–creatinine was defined at the time of blood sample collection using the CKD-EPI criteria. Comorbid diseases that represent potential confounders were defined using a comorbidity index calculated as the sum (score range, 0 to 8; converted to a percentage to account for missing data) of eight conditions: obesity, hypertension, diabetes, cancer, ischemic heart disease, chronic heart failure, chronic kidney disease, and chronic obstructive pulmonary disease (*3*).

Johns Hopkins CSF cohort

CSF and plasma samples from the same participants were used for proteomic analyses using SomaScan v4.1 assay (7288 SOMAmer reagents). Samples that did not pass SomaScan QC criteria were excluded (CSF, $n = 0$; plasma, $n = 2$). Samples identified as outliers by SomaScan or by principal components analyses were excluded (CSF, $n = 3$; plasma, $n = 1$). CVs were calculated using QC-pooled, matrix-matched sample replicates provided by SomaLogic to monitor overall assay performance. The paired plasma-CSF study design spanned three plates for each biological matrix (plasma or CSF) and included three matrix-matched QC sample replicates in each plate. CVs were calculated as CV = 100 × SD(RFU)/mean(RFU), where RFU is the SOMAmer intensity in relative fluorescence units measured for all intra- and interplate QC samples. Aptamers with CVs of >50% were excluded (CSF, $n = 15$; plasma, $n = 18$). The median CV for candidate protein plasma aptamers used in the current analyses was 5.8% for CSF and 4.0% for plasma. Values were $\log_2$ transformed, and those beyond 5 SDs were winsorized. Entrez Gene IDs were used as labels for corresponding aptamers.

GenS study

We used previously published results from the GenS: The Scottish Family Health Study, a population-based cohort that enrolled over 24,000 Scottish individuals between 2006 and 2011, including 1065 participants with proteomic and cognitive measurements collected concurrently at their clinical visit (*26*). Proteins were measured using the SomaScan v4.0 assay (4991 SOMAmer reagents), and performance was measured using six cognitive domains. Memory was computed as the sum of Immediate and delayed recall of one oral story from the Wechsler Logical Memory Test, where details correctly recalled about the story were recorded as points. Verbal fluency was assessed using the Controlled Oral Word Association Test (letters C, F, and L), reflecting the number of words named with a 1 min. Vocabulary was measured using the Mill Hill Vocabulary test. Processing speed was measured using the Wechsler Digit Symbol Substitution Task, specifically counts of correct pairs of digits recoded to symbols over 2 min. Nonverbal reasoning was assessed using the matrix reasoning test, which reflected the number of correct answers identifying missing elements in patterns presented as matrices. A measure of general cognition was computed as the first unrotated principal component combining logical memory, verbal fluency, processing speed, and vocabulary.

ARIC study

ARIC is a prospective epidemiologic study conducted in Forsyth County (NC) and Jackson (MS); the northwest suburbs of Minneapolis (MN) and Washington County (MD). The study enrolled 15,792 mostly white and Black participants aged 45 to 64 between 1987 and 1989 (*69*). Participants had four additional in-person visits after enrollment: visit 2 (1990–1992), visit 3 (1993–1995), visit 4 (1996–1999), and visit 5 (2011–2013). Additional follow-up visits are ongoing. Blood was drawn for proteomic analysis at visits 2 and visit 5. Mid-life (20-year) dementia risk was assessed between visit 2 and visit 5, and Aβ PET scans were acquired on a subset of participants at visit 5. Proteins were measured in ARIC using the SomaScan v4.0 assay (4991 SOMAmer reagents), as previously described (*70*). Values were $\log_2$ transformed, and those beyond 5 SDs were winsorized. Using 197 blind duplicates, the median CV for the aptamer examined in the current analyses (IGDCC4) was 8.4% at visit 2 and 5.1% at visit 5. ^{18}F-florbetapir PET scans (20 min) were acquired on Siemens scanners (various models across ARIC sites) 50 to 70 min after an intravenous bolus injection of the radiotracer, as described previously (*71*). SUVRs were calculated using cerebellar gray matter region as a reference. Mean cortical Aβ reflected average SUVR values across the orbitofrontal, prefrontal, and superior frontal cortices; lateral temporal, parietal, and occipital lobes, precuneus; and anterior and posterior cingulate ROIs. Aβ status (+/−) was defined on the basis of a median of 1.20 mean cortical SUVR. Dementia diagnosis was adjudicated through a cognitive and functional assessment (visit 5), telephone

screening, informant ratings, hospital records, and death record review, as previously described (*72*). At ARIC visits 2 and 4, a three-instrument cognitive assessment was applied (delayed word recall task, digit symbol substitution from the Wechsler Adult Intelligence Scale-Revised, and a letter fluency task). At ARIC visit 5, participants received a comprehensive cognitive exam and a functional assessment that included the Clinical Dementia Rating Scale and Functional Activities Questionnaire. Dementia was adjudicated by an expert panel of physicians and specialists and was based on the criteria outlined in the National Institute on Aging and Alzheimer's Association and the *Diagnostic and Statistical Manual of Mental Disorder*, Fifth Edition.

UK Biobank

Blood was drawn for proteomic and antigen-specific antibody analyses at study enrollment. Proteins were measured using the Olink Explore 3072 platform (2923 unique proteins), as described previously (*29*). Proteomic data preprocessing followed standard UKB QC procedures, where normalized protein expression values below the lower limits of detection were retained. The median CV for the protein examined in the current analyses (IGDCC4) was 5.4%. Log_2-transformed values were used in analyses. Long-term (14-year) dementia risk was assessed between 2007 and 2022. Dementia was ascertained with linked hospital discharge records, primary care records, and death certificates using diagnostic codes for ACD, AD, VaD, frontotemporal dementia, and Parkinson's disease dementia (table S41). Ascertainment of hypertension and type II diabetes (statistical covariates in dementia risk analyses) were derived from the GEMINI project (*73*). Antigen-specific antibody measurements were obtained from a multiplex glutathione *S*-transferase capture assay that used viral proteins generated from *Escherichia coli* conjugated to polystyrene beads (*74*); standardized values were used in analyses.

Religious Orders Study/Rush Memory and Aging Project

ROSMAP are two continuously enrolling community-based cohort studies, ROS across the USA and MAP across northeastern Illinois (*75*). All participants enrolled without known dementia agree to annual detailed clinical evaluations or brain donation at death. Annual study visits use complete clinical and functional evaluations, including medical history reports, cognitive assessments, and blood draws. Proteins were measured using the SomaScan v4.1 assay (7288 SOMAmer reagents), as described previously (*76*). Antibody titers were measured from blood drawn at the same study visit using the same assays as described in the BLSA.

Two-sample MR

Plasma pQTLs were obtained from a deCODE Genetics GWAS of SomaScan plasma protein levels ($n = 35{,}559$) (*21*); we included only pQTLs that met a genome-wide significance P value of 1.8×10^{-9}. CSF pQTLs were obtained from a WashU GWAS of SomaScan CSF protein levels ($n = 3107$) (*28*); we included only pQTLs with a genome-wide significance P value of 5×10^{-8}. Plasma or CSF pQTLs were used as genetic instruments. For outcomes, we used two GWAS of AD, one GWAS of ACD, five GWAS of brain aging neuroimaging signatures, and one GWAS of AD brain neuroimaging signatures. AD GWAS were derived from the EADB ($n = 487{,}511$; cases = 39,106) and the FinnGen project ($n = 214{,}893$; cases = 3899) (*22*, *23*). An ACD GWAS were derived from FinnGen ($n = 211{,}397$; cases = 7395) (*22*). GWAS of machine learning–based brain aging and AD brain imaging signatures were derived from the UKB ($n = 33{,}541$), as previously described (*25*, *77*, *78*). Briefly, these neuroimaging signatures capture the coexpression of multidimensional atrophy patterns characteristic of aging and AD; in large, multicohort studies, these machine learning–derived measures of aging- and AD-related brain atrophy predict age-related clinical traits and neurodegenerative disease risk, including clinical progression and dementia diagnosis (*25*, *77*, *78*). pQTLs were pruned to remove genetic variants in linkage disequilibrium ($r^2 < 0.05$) with the 1000 Genomes Project (European) as the reference panel. The random-effects inverse variance–weighted estimate (for proteins with multiple genetic instruments) or the Wald ratio estimate (for proteins with a single genetic instrumental variable) were considered for primary analyses. Sensitivity analyses were performed to assess the violation of MR assumptions using the MR Egger, simple mode, weighted median, weighted mode, and the Raw MR-PRESSO tests. Among proteins with sufficient numbers of available instruments, heterogeneity between causal estimates was tested using Cochran's Q (MR Egger and inverse variance–weighted) and the MR-PRESSO global test, and horizontal pleiotropy assumptions were tested using the MR Egger intercept. If heterogeneity assumptions were violated using inverse variance–weighted estimates, then MR Egger estimates were considered for primary analyses, and vice versa. If heterogeneity assumptions for both MR Egger and inverse variance–weighted estimates were violated, then MR-PRESSO raw estimates were considered for primary analyses. One SNP (rs10922098) was excluded from analyses because it was a plasma pQTL for three proteins, indicating associations that are likely a result of horizontal pleiotropy. MR analyses were performed using the TwoSampleMR (0.6.4), MendelianRandomization (0.10.0), and MR-PRESSO (1.0) R packages.

Biological characterization

A variety of complementary analytic tools, techniques, and open-source databases were used to understand the biological implications and functional relevance of plasma proteins. Enriched biological pathways were primarily identified using ingenuity pathway analysis (QIAGEN Inc.; version 01-22-01), a bioinformatics application that facilitates the analyses and interpretation of "-omics" data using curated content available via the Ingenuity Knowledge Base (IKB) (*79*). Proteins were mapped to the IKB using Entrez Gene symbols of the cognate genes encoding each protein. Differential expression patterns reflected associations with each viral antibody titer. The user dataset was used as the reference set (i.e., the population of genes considered for P value calculations was limited to those contained on the SomaScan platform), and direct and indirect relationships were considered. Benjamini-Hochberg FDR-adjusted P values derived from Fisher's exact tests quantified the probability of overlap between cognate genes encoding proteins and molecules known to exist within a specific pathway due to random chance. Cell-specific enrichment was primarily identified using Tabula Sapiens via the Enrichr platform (https://maayanlab.cloud/Enrichr/) (*80*). This human cell atlas of nearly 500,000 cells from 24 organs of 15 normal human participants was made available through the Tabula Sapiens Consortium. Benjamini-Hochberg FDR-adjusted P values derived from Fisher's exact tests quantified the probability of overlap between cognate genes encoding proteins and genes known to exist within a specific cell type due to random chance. The combined scores reflected the product of P values (log-transformed) from Fisher's exact tests multiplied by the z-scores of the deviations from each gene's expected

rank, which were derived from randomly imputed gene sets for each term. Additional cell-specific enrichment was identified using the PanglaoDB platform (https://panglaodb.se) (*81*). This atlas of over 4 million cells leverages over 1054 single-cell RNA-seq studies from National Center for Biotechnology Information's Sequence Read Archive, encompasses 155 unique cell types, and was made available through the Cardio Metabolic Center at the Karolinska Institute. Benjamini-Hochberg FDR-adjusted *P* values derived from Fisher's exact tests quantified the probability of overlap between cognate genes encoding proteins and gene known to exist within a specific cell cluster due to random chance. Tissue-specific enrichment used published findings that mapped organ-specific proteomes using human organ bulk RNA-seq data from the Genotype-Tissue Expression project (https://gtexportal.org/home/), where a cognate gene encoding a plasma protein was considered enriched if it was expressed at least four times higher in a single organ (or groups of organs) compared to any other organ (*82*). Studies (i.e., PubMed IDs) were identified that externally validated SOMAmer reagents using one or more of the following techniques: multiple reaction monitoring mass spectroscopy (which determines protein content in a single sample after SOMAmer enrichment) and data-dependent analysis mass spectroscopy [which determines protein content after SOMAmer enrichment for pull-down testing in matrix (e.g., plasma)], pQTLs (which indicate that genetic strategies, such as cis-pQTL associations, directly link a gene to a protein and a SOMAmer), orthogonal strategies (which refer to variety of methods that used SOMAmer reagent–independent techniques to quantify and confirm protein identity and level of expression, including enzyme-linked immunosorbent assay, histochemistry, Western blot, particle-based immunoassay, etc.), and proximity extension assays (which use antibody pairs conjugated to unique oligonucleotides and quantitative PCR to determine that protein levels in plasma and SOMAmers display correlations of >0.40). For comparative gene expression across 76 cell types, we used consensus transcript expression levels from the Human Protein Atlas (www.proteinatlas.org/about/), where a given gene was considered highly expressed in a cell type if that cell type was among the top five cells with the highest expression of the given gene. Similarly, for comparative gene expression across 54 tissue types, we used consensus transcript expression levels from the Human Protein Atlas, where a given gene was considered highly expressed in a tissue type if that tissue type was among the top five tissues with the highest expression of the given gene. Protein interaction networks were assessed using STRING (Search Tool for the Retrieval of Interacting Genes/Proteins) (https://string-db.org), a database and visualization tool that integrates publicly available sources of information to provide a comprehensive understanding of protein-protein interaction (PPI) networks (*83*). PPI *P* values derived from an explicit null model to account for the non-uniform distribution of the connectivity degrees of network proteins (i.e., a random graph with given degree sequence model) reflected the likelihood of proteins having more interactions among themselves than what would be expected for a random set of proteins of the same size drawn from the genome, suggesting if the proteins are at least partially biologically connected as a group. STRING was also used to assess enriched biological processed via open-source databases (e.g., Gene Ontology, Kyoto Encyclopedia of Genes and Genomes, WikiPathways, etc.). RNA-seq expression across six prominent CNS cell types (excitatory neurons, inhibitory neurons, oligodendrocytes, astrocytes, oligodendrocyte precursor cells, and microglia) in prefrontal cortex tissue of patients with AD was obtained from previously published results derived from participants in the ROSMAP ($n = 48$) (*84*). Here, early pathology was defined as some amyloid burden, modest neurofibrillary tangles, and modest cognitive impairment; late pathology was defined as high amyloid burden, high neurofibrillary tangles, high global pathology, and moderate/severe cognitive impairment. RNA-seq expression in neurovasculature cell types (AD = 13 and control = 12) was obtained from the Human BBB (https://twc-stanford.shinyapps.io/human_bbb/), a transcriptomic dataset generated using VINE (Vessel Isolation and Nuclei Extraction) RNA-seq (*85*). Hippocampal tissue of 5-month-old 5xFAD ($n = 6$) and wild-type ($n = 6$) mice was used for mass spectrometry proteomics (label-free quantification) (*86*). Hippocampal tissue of 10-month- old APP/PS1 ($n = 12$) and wild-type ($n = 12$) mice was used for bulk RNA-seq (*87*).

Statistical analyses

Logistic regression models adjusting for age, sex, race, education, *APOEε4* status, sample storage time, and a comorbidity index were used to examine associations of antibody levels with odds of dementia and Aβ+ PET status. Linear regression models adjusting for the aforementioned covariates were used to examine associations with domain-specific cognitive performance, 3-T MRI–derived brain volumes, estimated age of Aβ+ onset, mean cortical Aβ level, ADRD plasma biomarkers, and the plasma proteome. Model quality and goodness of fit were assessed using the performance R package (0.11.0.8) and visual inspection (e.g., residual distributions, Q-Q plots, etc.). Brain volume analyses also adjusted for intracranial volume. Plasma biomarker and proteomic analyses additionally adjusted for eGFR. Mean cortical Aβ was only examined as an outcome in Aβ+ participants because PiB PET in the presence of low or absent Aβ can reflect tracer kinetics rather than Aβ deposition (*88*). Given a limited sample size, linear regression adjusting for age, sex, Aβ PET status, and a comorbidity index were used to examine associations with tau PET. A two-way interaction term was incorporated into models to examine effect modification by self-reported sex. Proteins measured in GenS were related to cognitive domain performance using linear mixed-effects models adjusting for relatedness between individuals (i.e., kinship matrix), age, sex, depression diagnosis, clinic study site, and sample storage time. Proteins measured in ARIC were related to incident dementia risk using Cox proportional hazards regression models adjusting for age, sex, race-center, education, *APOEε4*, eGFR, and cardiovascular risk factors [body mass index (BMI), diabetes, hypertension, and current smoking status]. Logistic regression models adjusting for the aforementioned covariates were used to examine associations with Aβ+ PET status. Proteins measured in UKB were related to incident dementia risk using Cox proportional hazards regression models adjusting age, sex, education, study site, *APOEε4*, eGFR and cardiovascular risk factors (BMI, diabetes, hypertension, and current smoking status) and related to antigen measurements using linear regression models adjusted for age, sex, and BMI. Welch's *t* test was used to compare expression levels between AD and healthy controls across neurovascular cell types. Statistical significance was defined at two-sided $P < 0.05$. Analyses were performed using R (version 4.2.2) and SAS (version 9.4). Graphs were generated in R and the BioRender platform (www.biorender.com).

Study approval

All studies were conducted in accordance with the Declaration of Helsinki. The BLSA protocol was approved by the Institutional Review Board (IRB) of the National Institute of Environmental Health Science,

National Institutes of Health (03AG0325), and the BLSA PET studies were additionally approved by the Johns Hopkins University Medicine IRB. All BLSA participants gave informed consent before participation. Participants referred to the Johns Hopkins Hospital Neurology Clinic consented to banking of residual CSF after clinical testing under an IRB-approved protocol. GenS received approval from the NHS (National Health Service) Tayside Committee on Medical Research Ethics (05/S1401/89) and the East of Scotland Research Ethics Service (20/ES/0021); all participants provided informed consent. Informed consent was obtained for all ARIC participants, and protocols were approved by IRBs at participating centers. The UKB study was approved by the NHS National Research Ethics Service (11/NW/0382), and all participants gave informed consent. ROSMAP was approved by an IRB at Rush University Medical Center (L91020181 and L86121802), and all participants signed an informed consent, Anatomical Gift Act, and a Rush Alzheimer's Disease Center Repository consent (L99032481).

Supplementary Materials

The PDF file includes:
Figs. S1 to S8
Legends for tables S1 to S41

Other Supplementary Material for this manuscript includes the following:
Tables S1 to S41

REFERENCES AND NOTES

1. B. M. Bettcher, M. G. Tansey, G. Dorothée, M. T. Heneka, Peripheral and central immune system crosstalk in Alzheimer disease - A research prospectus. *Nat. Rev. Neurol.* **17**, 689–701 (2021).
2. K. A. Walker, L. M. Le Page, N. Terrando, M. R. Duggan, M. T. Heneka, B. M. Bettcher, The role of peripheral inflammatory insults in Alzheimer's disease: A review and research roadmap. *Mol. Neurodegener.* **18**, 37 (2023).
3. M. R. Duggan, Z. Peng, Y. An, M. H. Kitner Triolo, A. T. Shafer, C. Davatzikos, G. Erus, A. Karikkineth, A. Lewis, A. Moghekar, K. A. Walker, Herpes viruses in the Baltimore Longitudinal Study of Aging: Associations with brain volumes, cognitive performance, and plasma biomarkers. *Neurology* **99**, e2014–e2024 (2022).
4. P. N. Sipilä, N. Heikkilä, J. V. Lindbohm, C. Hakulinen, J. Vahtera, M. Elovainio, S. Suominen, A. Väänänen, A. Koskinen, S. T. Nyberg, J. Pentti, T. E. Strandberg, M. Kivimäki, Hospital-treated infectious diseases and the risk of dementia: A large, multicohort, observational study with a replication cohort. *Lancet Infect. Dis.* **21**, 1557–1567 (2021).
5. R. Muzambi, K. Bhaskaran, L. Smeeth, C. Brayne, N. Chaturvedi, C. Warren-Gash, Assessment of common infections and incident dementia using UK primary and secondary care data: A historical cohort study. *Lancet Healthy Longev.* **2**, e426–e435 (2021).
6. M. R. Duggan, Z. Peng, P. N. Sipilä, J. V. Lindbohm, J. Chen, Y. Lu, C. Davatzikos, G. Erus, T. J. Hohman, S. J. Andrews, J. Candia, T. Tanaka, C. M. Joynes, C. X. Alvarado, M. A. Nalls, J. Cordon, G. N. Daya, Y. An, A. Lewis, A. Moghekar, P. Palta, J. Coresh, L. Ferrucci, M. Kivimäki, K. A. Walker, Proteomics identifies potential immunological drivers of postinfection brain atrophy and cognitive decline. *Nat. Aging* **4**, 1263–1278 (2024).
7. R. Mancuso, F. Baglio, M. Cabinio, E. Calabrese, A. Hernis, R. Nemni, M. Clerici, Titers of herpes simplex virus type 1 antibodies positively correlate with grey matter volumes in Alzheimer's disease. *J. Alzheimers Dis.* **38**, 741–745 (2013).
8. S. Agostini, R. Mancuso, F. Baglio, M. Cabinio, A. Hernis, A. S. Costa, E. Calabrese, R. Nemni, M. Clerici, High avidity HSV-1 antibodies correlate with absence of amnestic mild cognitive impairment conversion to Alzheimer's disease. *Brain Behav. Immun.* **58**, 254–260 (2016).
9. R. E. Green, C. H. Sudre, C. Warren-Gash, J. Butt, T. Waterboer, A. D. Hughes, J. M. Schott, M. Richards, N. Chaturvedi, D. M. Williams, Common infections and neuroimaging markers of dementia in three UK cohort studies. *Alzheimers Dement.* **20**, 2128–2142 (2024).
10. G. Westman, J. Blomberg, Z. Yun, L. Lannfelt, M. Ingelsson, B. M. Eriksson, Decreased HHV-6 IgG in Alzheimer's disease. *Front. Neurol.* **8**, 40 (2017).
11. S. Agostini, R. Mancuso, A. Hernis, A. S. Costa, R. Nemni, M. Clerici, HSV-1-specific IgG subclasses distribution and serum neutralizing activity in Alzheimer's disease and in mild cognitive impairment. *J. Alzheimers Dis.* **63**, 131–138 (2018).
12. X. Wu, H. Yang, S. He, T. Xia, D. Chen, Y. Zhou, J. Liu, M. Liu, Z. Sun, Adult vaccination as a protective factor for dementia: A meta-analysis and systematic review of population-based observational studies. *Front. Immunol.* **13**, 872542 (2022).
13. K. A. Walker, B. N. Ficek, R. Westbrook, Understanding the role of systemic inflammation in Alzheimer's disease. *ACS Chem. Neurosci.* **10**, 3340–3342 (2019).
14. J. V. Pluvinage, T. Wyss-Coray, Systemic factors as mediators of brain homeostasis, ageing and neurodegeneration. *Nat. Rev. Neurosci.* **21**, 93–102 (2020).
15. C. Greene, R. Connolly, D. Brennan, A. Laffan, E. O'Keeffe, L. Zaporojan, J. O'Callaghan, B. Thomson, E. Connolly, R. Argue, J. F. M. Meaney, I. Martin-Loeches, A. Long, C. N. Cheallaigh, N. Conlon, C. P. Doherty, M. Campbell, Blood–brain barrier disruption and sustained systemic inflammation in individuals with long COVID-associated cognitive impairment. *Nat. Neurosci.* **27**, 421–432 (2024).
16. M. A. Beydoun, H. A. Beydoun, N. Noren Hooten, O. Meirelles, Z. Li, Z. W. El-Hajj, J. Weiss, C. A. Maino Vieytes, L. J. Launer, M. K. Evans, A. B. Zonderman, Hospital-treated prevalent infections, the plasma proteome and incident dementia among UK older adults. *iScience* **26**, 108526 (2023).
17. K. A. Walker, J. Chen, L. Shi, Y. Yang, M. Fornage, L. Zhou, P. Schlosser, A. Surapaneni, M. E. Grams, M. R. Duggan, Z. Peng, G. T. Gomez, A. Tin, R. C. Hoogeveen, K. J. Sullivan, P. Ganz, J. V. Lindbohm, M. Kivimaki, A. J. Nevado-Holgado, N. Buckley, R. F. Gottesman, T. H. Mosley, E. Boerwinkle, C. M. Ballantyne, J. Coresh, Proteomics analysis of plasma from middle-aged adults identifies protein markers of dementia risk in later life. *Sci. Transl. Med.* **15**, eadf5681 (2023).
18. S. Morgello, Coronaviruses and the central nervous system. *J. Neurovirol.* **26**, 459–473 (2020).
19. M. R. Duggan, B. Torkzaban, T. M. Ahooyi, K. Khalili, Potential role for herpesviruses in Alzheimer's disease. *J. Alzheimers Dis.* **78**, 855–869 (2020).
20. E. G. Severance, I. Bossis, F. B. Dickerson, C. R. Stallings, A. E. Origoni, A. Sullens, R. H. Yolken, R. P. Viscidi, Development of a nucleocapsid-based human coronavirus immunoassay and estimates of individuals exposed to coronavirus in a U.S. metropolitan population. *Clin. Vaccine Immunol.* **15**, 1805–1810 (2008).
21. E. Ferkingstad, P. Sulem, B. A. Atlason, G. Sveinbjornsson, M. I. Magnusson, E. L. Styrmisdottir, K. Gunnarsdottir, A. Helgason, A. Oddsson, B. V. Halldorsson, B. O. Jensson, F. Zink, G. H. Halldorsson, G. Masson, G. A. Arnadottir, H. Katrinardottir, K. Juliusson, M. K. Magnusson, O. T. Magnusson, R. Fridriksdottir, S. Saevarsdottir, S. A. Gudjonsson, S. N. Stacey, S. Rognvaldsson, T. Eiriksdottir, T. A. Olafsdottir, V. Steinthorsdottir, V. Tragante, M. O. Ulfarsson, H. Stefansson, I. Jonsdottir, H. Holm, T. Rafnar, P. Melsted, J. Saemundsdottir, G. L. Norddahl, S. H. Lund, D. F. Gudbjartsson, U. Thorsteinsdottir, K. Stefansson, Large-scale integration of the plasma proteome with genetics and disease. *Nat. Genet.* **53**, 1712–1721 (2021).
22. M. I. Kurki, J. Karjalainen, P. Palta, T. P. Sipilä, K. Kristiansson, K. M. Donner, M. P. Reeve, H. Laivuori, M. Aavikko, M. A. Kaunisto, A. Loukola, E. Lahtela, H. Mattsson, P. Laiho, P. D. B. Parolo, A. A. Lehisto, M. Kanai, N. Mars, J. Rämö, T. Kiiskinen, H. O. Heyne, K. Veerapen, S. Rüeger, S. Lemmelä, W. Zhou, S. Ruotsalainen, K. Pärn, T. Hiekkalinna, S. Koskelainen, T. Paajanen, V. Llorens, J. Gracia-Tabuenca, H. Siirtola, K. Reis, A. G. Elnahas, B. Sun, C. N. Foley, K. Aalto-Setälä, K. Alasoo, M. Arvas, K. Auro, S. Biswas, A. Bizaki-Vallaskangas, O. Carpen, C.-Y. Chen, O. A. Dada, Z. Ding, M. G. Ehm, K. Eklund, M. Färkkilä, H. Finucane, A. Ganna, A. Ghazal, R. R. Graham, E. M. Green, A. Hakanen, M. Hautalahti, Å. K. Hedman, M. Hiltunen, R. Hinttala, I. Hovatta, X. Hu, A. Huertas-Vazquez, L. Huilaja, J. Hunkapiller, H. Jacob, J.-N. Jensen, H. Joensuu, S. John, V. Julkunen, M. Jung, J. Junttila, K. Kaarniranta, M. Kähönen, R. Kajanne, L. Kallio, R. Kälviäinen, J. Kaprio, FinnGen, N. Kerimov, J. Kettunen, E. Kilpeläinen, T. Kilpi, K. Klinger, V.-M. Kosma, T. Kuopio, V. Kurra, T. Laisk, J. Laukkanen, N. Lawless, A. Liu, S. Longerich, R. Mägi, J. Mäkelä, A. Mäkitie, A. Malarstig, A. Mannermaa, J. Maranville, A. Matakidou, T. Meretoja, S. V. Mozaffari, M. E. K. Niemi, M. Niemi, T. Niiranen, C. J. O'Donnell, M. Obeidat, G. Okafo, H. M. Ollila, A. Palomäki, T. Palotie, J. Partanen, D. S. Paul, M. Pelkonen, R. K. Pendergrass, S. Petrovski, A. Pitkäranta, A. Platt, D. Pulford, E. Punkka, P. Pussinen, N. Raghavan, F. Rahimov, D. Rajpal, N. A. Renaud, B. Riley-Gillis, R. Rodosthenous, E. Saarentaus, A. Salminen, E. Salminen, V. Salomaa, J. Schleutker, R. Serpi, H.-y. Shen, R. Siegel, K. Silander, S. Siltanen, S. Soini, H. Soininen, J. H. Sul, I. Tachmazidou, K. Tasanen, P. Tienari, S. Toppila-Salmi, T. Tukiainen, T. Tuomi, J. A. Turunen, J. C. Ulirsch, F. Vaura, P. Virolainen, J. Waring, D. Waterworth, R. Yang, M. Nelis, A. Reigo, A. Metspalu, L. Milani, T. Esko, C. Fox, A. S. Havulinna, M. Perola, S. Ripatti, A. Jalanko, T. Laitinen, T. P. Mäkelä, R. Plenge, M. M. Carthy, H. Runz, M. J. Daly, A. Palotie, FinnGen provides genetic insights from a well-phenotyped isolated population. *Nature* **613**, 508–518 (2023).
23. C. Bellenguez, F. Küçükali, I. E. Jansen, L. Kleineidam, S. Moreno-Grau, N. Amin, A. C. Naj, R. Campos-Martin, B. Grenier-Boley, V. Andrade, P. A. Holmans, A. Boland, V. Damotte, S. J. van der Lee, M. R. Costa, T. Kuulasmaa, Q. Yang, I. de Rojas, J. C. Bis, A. Yaqub, I. Prokic, J. Chapuis, S. Ahmad, V. Giedraitis, D. Aarsland, P. Garcia-Gonzalez, C. Abdelnour, E. Alarcón-Martín, D. Alcolea, M. Alegret, I. Alvarez, V. Álvarez, N. J. Armstrong, A. Tsolaki, C. Antúnez, I. Appollonio, M. Arcaro, S. Archetti, A. A. Pastor, B. Arosio, L. Athanasiu, H. Bailly, N. Banaj, M. Baquero, S. Barral, A. Beiser, A. B. Pastor, J. E. Below, P. Benchek,

L. Benussi, C. Berr, C. Besse, V. Bessi, G. Binetti, A. Bizarro, R. Blesa, M. Boada, E. Boerwinkle, B. Borroni, S. Boschi, P. Bossù, G. Bråthen, J. Bressler, C. Bresner, H. Brodaty, K. J. Brookes, L. I. Brusco, D. Buiza-Rueda, K. Bürger, V. Burholt, W. S. Bush, M. Calero, L. B. Cantwell, G. Chene, J. Chung, M. L. Cuccaro, Á. Carracedo, R. Cecchetti, L. Cervera-Carles, C. Charbonnier, H.-H. Chen, C. Chillotti, S. Ciccone, J. A. H. R. Claassen, C. Clark, E. Conti, A. Corma-Gómez, E. Costantini, C. Custodero, D. Daian, M. C. Dalmasso, A. Daniele, E. Dardiotis, J.-F. Dartigues, P. P. de Deyn, K. de Paiva Lopes, L. D. de Witte, S. Debette, J. Deckert, T. del Ser, N. Denning, A. De Stefano, M. Dichgans, J. Diehl-Schmid, M. Diez-Fairen, P. D. Rossi, S. Djurovic, E. Duron, E. Düzel, C. Dufouil, G. Eiriksdottir, S. Engelborghs, V. Escott-Price, A. Espinosa, M. Ewers, K. M. Faber, T. Fabrizio, S. F. Nielsen, D. W. Fardo, L. Farotti, C. Fenoglio, M. Fernández-Fuertes, R. Ferrari, C. B. Ferreira, E. Ferri, B. Fin, P. Fischer, T. Fladby, K. Fließbach, B. Fongang, M. Fornage, J. Fortea, T. M. Foroud, S. Fostinelli, N. C. Fox, E. Franco-Macías, M. J. Bullido, A. Frank-García, L. Froelich, B. Fulton-Howard, D. Galimberti, J. M. García-Alberca, P. García-González, S. Garcia-Madrona, G. Garcia-Ribas, R. Ghidoni, I. Giegling, G. Giorgio, A. M. Goate, O. Goldhardt, D. Gomez-Fonseca, A. González-Pérez, C. Graff, G. Grande, E. Green, T. Grimmer, E. Grünblatt, M. Grunin, V. Gudnason, T. Guetta-Baranes, A. Haapasalo, G. Hadjigeorgiou, J. L. Haines, K. L. Hamilton-Nelson, H. Hampel, O. Hanon, J. Hardy, A. M. Hartmann, L. Hausner, J. Harwood, S. Heilmann-Heimbach, S. Helisalmi, M. T. Heneka, I. Hernández, M. J. Herrmann, P. Hoffmann, C. Holmes, H. Holstege, R. H. Vilas, M. Hulsman, J. Humphrey, G. J. Biessels, X. Jian, C. Johansson, G. R. Jun, Y. Kastumata, J. Kauwe, P. G. Kehoe, L. Kilander, A. K. Ståhlbom, M. Kivipelto, A. Koivisto, J. Kornhuber, M. H. Kosmidis, W. A. Kukull, P. P. Kuksa, B. W. Kunkle, A. B. Kuzma, C. Lage, E. J. Laukka, L. Launer, A. Lauria, C.-Y. Lee, J. Lehtisalo, O. Lerch, A. Lleó, W. L. Jr, O. Lopez, A. L. de Munain, S. Love, M. Löwemark, L. Luckcuck, K. L. Lunetta, Y. Ma, J. Macías, C. A. Mac Leod, W. Maier, F. Mangialasche, M. Spallazzi, M. Marquié, R. Marshall, E. R. Martin, A. M. Montes, C. M. Rodríguez, C. Masullo, R. Mayeux, S. Mead, P. Mecocci, M. Medina, A. Meggy, S. Mehrabian, S. Mendoza, M. Menéndez-González, P. Mir, S. Moebus, M. Mol, L. Molina-Porcel, L. Montrreal, L. Morelli, F. Moreno, K. Morgan, T. Mosley, M. M. Nöthen, C. Muchnik, S. Mukherjee, B. Nacmias, T. Ngandu, G. Nicolas, B. G. Nordestgaard, R. Olaso, A. Orellana, M. Orsini, G. Ortega, A. Padovani, C. Paolo, G. Papenberg, L. Parnetti, F. Pasquier, P. Pastor, G. Peloso, A. Pérez-Cordón, J. Pérez-Tur, P. Pericard, O. Peters, Y. A. L. Pijnenburg, J. A. Pineda, G. Piñol-Ripoll, C. Pisanu, T. Polak, J. Popp, D. Posthuma, J. Priller, R. Puerta, O. Quenez, I. Quintela, J. Q. Thomassen, A. Rábano, I. Rainero, F. Rajabli, I. Ramakers, L. M. Real, M. J. T. Reinders, C. Reitz, D. Reyes-Dumeyer, P. Ridge, S. Riedel-Heller, P. Riederer, N. Roberto, E. Rodriguez-Rodriguez, A. Rongve, I. R. Allende, M. Rosende-Roca, J. L. Royo, E. Rubino, D. Rujescu, M. E. Sáez, P. Sakka, I. Saltvedt, Á. Sanabria, M. B. Sánchez-Arjona, F. Sanchez-Garcia, P. S. Juan, R. Sánchez-Valle, S. B. Sando, C. Sarnowski, C. L. Satizabal, M. Scamosci, N. Scarmeas, E. Scarpini, P. Scheltens, N. Scherbaum, M. Scherer, M. Schmid, A. Schneider, J. M. Schott, G. Selbæk, D. Seripa, M. Serrano, J. Sha, A. A. Shadrin, O. Skrobot, S. Slifer, G. J. L. Snijders, H. Soininen, V. Solfrizzi, A. Solomon, Y. Song, S. Sorbi, O. Sotolongo-Grau, G. Spalletta, A. Spottke, A. Squassina, E. Stordal, J. P. Tartan, L. Tárraga, N. Tesí, A. Thalamuthu, T. Thomas, G. Tosto, L. Traykov, L. Tremolizzo, A. Tybjærg-Hansen, A. Uitterlinden, A. Ullgren, I. Ulstein, S. Valero, O. Valladares, C. Van Broeckhoven, J. Vance, B. N. Vardarajan, A. van der Lugt, J. Van Dongen, J. van Rooij, J. van Swieten, R. Vandenberghe, F. Verhey, J.-S. Vidal, J. Vogelgsang, M. Vyhnalek, M. Wagner, D. Wallon, L.-S. Wang, R. Wang, L. Weinhold, J. Wiltfang, G. Windle, B. Woods, M. Yannakoulia, H. Zare, Y. Zhao, X. Zhang, C. Zhu, M. Zulaica, EADB, GR@ACE, DEGESCO, EADI, GERAD, Demgene, FinnGen, ADGC, CHARGE, L. A. Farrer, B. M. Psaty, M. Ghanbari, T. Raj, P. Sachdev, K. Mather, F. Jessen, M. A. Ikram, A. de Mendonça, J. Hort, M. Tsolaki, M. A. Pericak-Vance, P. Amouyel, J. Williams, R. Frikke-Schmidt, J. Clarimon, J.-F. Deleuze, G. Rossi, S. Seshadri, O. A. Andreassen, M. Ingelsson, M. Hiltunen, K. Sleegers, G. D. Schellenberg, C. M. van Duijn, R. Sims, W. M. van der Flier, A. Ruiz, A. Ramirez, J.-C. Lambert, New insights into the genetic etiology of Alzheimer's disease and related dementias. *Nat. Genet.* **54**, 412–436 (2022).

24. Z. Yang, J. Wen, G. Erus, S. T. Govindarajan, R. Melhem, E. Mamourian, Y. Cui, D. Srinivasan, A. Abdulkadir, P. Parmpi, K. Wittfeld, H. J. Grabe, R. Bülow, S. Frenzel, D. Tosun, M. Bilgel, Y. An, D. Yi, D. S. Marcus, P. LaMontagne, T. L. S. Benzinger, S. R. Heckbert, T. R. Austin, S. R. Waldstein, M. K. Evans, A. B. Zonderman, L. J. Launer, A. Sotiras, M. A. Espeland, C. L. Masters, P. Maruff, J. Fripp, A. W. Toga, S. O'Bryant, M. M. Chakravarty, S. Villeneuve, S. C. Johnson, J. C. Morris, M. S. Albert, K. Yaffe, H. Völzke, L. Ferrucci, R. Nick Bryan, R. T. Shinohara, Y. Fan, M. Habes, P. A. Lalousis, N. Koutsouleris, D. A. Wolk, S. M. Resnick, H. Shou, I. M. Nasrallah, C. Davatzikos, Brain aging patterns in a large and diverse cohort of 49,482 individuals. *Nat. Med.* **30**, 3015–3026 (2024).
25. C. Davatzikos, F. Xu, Y. An, Y. Fan, S. M. Resnick, Longitudinal progression of Alzheimer's-like patterns of atrophy in normal older adults: The SPARE-AD index. *Brain* **132**, 2026–2035 (2009).
26. D. A. Gadd, R. F. Hillary, D. L. McCartney, L. Shi, A. Stolicyn, N. A. Robertson, R. M. Walker, R. I. McGeachan, A. Campbell, S. Xueyi, M. C. Barbu, C. Green, S. W. Morris, M. A. Harris, E. V. Backhouse, J. M. Wardlaw, J. D. Steele, D. A. Oyarzún, G. Muniz-Terrera, C. Ritchie, A. Nevado-Holgado, T. Chandra, C. Hayward, K. L. Evans, D. J. Porteous, S. R. Cox, H. C. Whalley, A. M. McIntosh, R. E. Marioni, Integrated methylome and phenome study of the circulating proteome reveals markers pertinent to brain health. *Nat. Commun.* **13**, 4670 (2022).
27. Q. He, W. Wang, Y. Xiong, C. Tao, L. Ma, C. You, Potential biomarkers in cerebrospinal fluid and plasma for dementia. *J. Alzheimers Dis.* **100**, 603–611 (2024).
28. C. Cruchaga, D. Western, J. Timsina, L. Wang, C. Wang, C. Yang, M. Ali, A. Beric, P. Gorijala, P. Kohlfeld, J. Budde, A. Levey, J. Morris, R. Perrin, A. Ruiz, M. Marquié, M. Boada, I. de Rojas, J. Rutledge, H. Oh, E. Wilson, Y. L. Guen, I. Alvarez, M. Aguilar, M. Greicius, P. Pastor, D. Pulford, L. Ibanez, T. Wyss-Coray, Y. J. Sung, B. Phillips, Proteogenomic analysis of human cerebrospinal fluid identifies neurologically relevant regulation and informs causal proteins for Alzheimer's disease. *Res. Sq.*, 10.21203/rs.3.rs-2814616/v1 (2023).
29. G. H. Eldjarn, E. Ferkingstad, S. H. Lund, H. Helgason, O. T. Magnusson, K. Gunnarsdottir, T. A. Olafsdottir, B. V. Halldorsson, P. I. Olason, F. Zink, S. A. Gudjonsson, G. Sveinbjornsson, M. I. Magnusson, A. Helgason, A. Oddsson, G. H. Halldorsson, M. K. Magnusson, S. Saevarsdottir, T. Eiriksdottir, G. Masson, H. Stefansson, I. Jonsdottir, H. Holm, T. Rafnar, P. Melsted, J. Saemundsdottir, G. L. Norddahl, G. Thorleifsson, M. O. Ulfarsson, D. F. Gudbjartsson, U. Thorsteinsdottir, P. Sulem, K. Stefansson, Large-scale plasma proteomics comparisons through genetics and disease associations. *Nature* **622**, 348–358 (2023).
30. L. Wang, D. Western, J. Timsina, C. Repaci, W.-M. Song, J. Norton, P. Kohlfeld, J. Budde, S. Climer, O. H. Butt, D. Jacobson, M. Garvin, A. R. Templeton, S. Campagna, J. O'Halloran, R. Presti, C. W. Goss, P. A. Mudd, B. M. Ances, B. Zhang, Y. J. Sung, C. Cruchaga, Plasma proteomics of SARS-CoV-2 infection and severity reveals impact on Alzheimer's and coronary disease pathways. *iScience* **26**, 106408 (2023).
31. I. Leshchyns'ka, V. Sytnyk, Reciprocal interactions between cell adhesion molecules of the immunoglobulin superfamily and the cytoskeleton in neurons. *Front. Cell Dev. Biol.* **4**, 9 (2016).
32. Y. Song, H. Huang, Y. Hu, J. Zhang, F. Li, X. Yin, J. Shi, Y. Li, C. Li, D. Zhao, H. Chen, A genome-wide CRISPR/Cas9 gene knockout screen identifies immunoglobulin superfamily DCC subclass member 4 as a key host factor that promotes influenza virus endocytosis. *PLOS Pathog.* **17**, e1010141 (2021).
33. R. H. Elhalag, K. R. Motawea, N. E. Talat, S. S. Rouzan, N. Mahmoud, E. M. Hammad, S. M. Reyad, M. S. Mohamed, J. Shah, Herpes simplex virus infection and the risk of dementia: A systematic review and meta-analysis. *Ann. Med. Surg.* **85**, 5060–5074 (2023).
34. C. Warren-Gash, H. J. Forbes, E. Williamson, J. Breuer, A. C. Hayward, A. Mavrodaris, B. H. Ridha, M. N. Rossor, S. L. Thomas, L. Smeeth, Human herpesvirus infections and dementia or mild cognitive impairment: A systematic review and meta-analysis. *Sci. Rep.* **9**, 4743 (2019).
35. S. E. Marsh, E. M. Abud, A. Lakatos, A. Karimzadeh, S. T. Yeung, H. Davtyan, G. M. Fote, L. Lau, J. G. Weinger, T. E. Lane, M. A. Inlay, W. W. Poon, M. Blurton-Jones, The adaptive immune system restrains Alzheimer's disease pathogenesis by modulating microglial function. *Proc. Natl. Acad. Sci. U.S.A.* **113**, E1316–E1325 (2016).
36. H. Scholtzova, E. Do, S. Dhakal, Y. Sun, S. Liu, P. D. Mehta, T. Wisniewski, Innate immunity stimulation via toll-like receptor 9 ameliorates vascular amyloid pathology in Tg-SwDI mice with associated cognitive benefits. *J. Neurosci.* **37**, 936–959 (2017).
37. K. L. Patrick, S. L. Bell, C. G. Weindel, R. O. Watson, Exploring the "multiple-hit hypothesis" of neurodegenerative disease: Bacterial infection comes up to bat. *Front. Cell. Infect. Microbiol.* **9**, 138 (2019).
38. J. V. Lindbohm, N. Mars, P. N. Sipilä, A. Singh-Manoux, H. Runz, FinnGen, G. Livingston, S. Seshadri, R. Xavier, A. D. Hingorani, S. Ripatti, M. Kivimäki, Immune system-wide Mendelian randomization and triangulation analyses support autoimmunity as a modifiable component in dementia-causing diseases. *Nat. Aging* **2**, 956–972 (2022).
39. A. C. Wendeln, K. Degenhardt, L. Kaurani, M. Gertig, T. Ulas, G. Jain, J. Wagner, L. M. Häsler, K. Wild, A. Skodras, T. Blank, O. Staszewski, M. Datta, T. P. Centeno, V. Capece, M. R. Islam, C. Kerimoglu, M. Staufenbiel, J. L. Schultze, M. Beyer, M. Prinz, M. Jucker, A. Fischer, J. J. Neher, Innate immune memory in the brain shapes neurological disease hallmarks. *Nature* **556**, 332–338 (2018).
40. E. Morenas-Rodríguez, Y. Li, B. Nuscher, N. Franzmeier, C. Xiong, M. Suárez-Calvet, A. M. Fagan, S. Schultz, B. A. Gordon, T. L. S. Benzinger, J. Hassenstab, E. McDade, R. Feederle, C. M. Karch, K. Schlepckow, J. C. Morris, G. Kleinberger, B. Nellgard, J. Vöglein, K. Blennow, H. Zetterberg, M. Ewers, M. Jucker, J. Levin, R. J. Bateman, C. Haass, Dominantly Inherited Alzheimer Network, Soluble TREM2 in CSF and its association with other biomarkers and cognition in autosomal-dominant Alzheimer's disease: A longitudinal observational study. *Lancet Neurol.* **21**, 329–341 (2022).
41. Z. Fan, D. J. Brooks, A. Okello, P. Edison, An early and late peak in microglial activation in Alzheimer's disease trajectory. *Brain* **140**, 792–803 (2017).
42. S. Ghosh, M. D. Wu, S. S. Shaftel, S. Kyrkanides, F. M. LaFerla, J. A. Olschowka, M. K. O'Banion, Sustained interleukin-1β overexpression exacerbates tau pathology despite reduced amyloid burden in an Alzheimer's mouse model. *J. Neurosci.* **33**, 5053–5064 (2013).
43. W. A. Eimer, D. K. Vijaya Kumar, N. K. Navalpur Shanmugam, A. S. Rodriguez, T. Mitchell, K. J. Washicosky, B. György, X. O. Breakefield, R. E. Tanzi, R. D. Moir, Alzheimer's

disease-associated β-amyloid is rapidly seeded by herpesviridae to protect against brain infection. *Neuron* **99**, 56–63.e3 (2018).
44. M. Desforges, A. Le Coupanec, P. Dubeau, A. Bourgouin, L. Lajoie, M. Dubé, P. J. Talbot, Human coronaviruses and other respiratory viruses: Underestimated opportunistic pathogens of the central nervous system? *Viruses* **12**, 14 (2020).
45. R. P. dos Santos Alves, J. Timis, R. Miller, K. Valentine, P. B. A. Pinto, A. Gonzalez, J. A. Regla-Nava, E. Maule, M. N. Nguyen, N. Shafee, S. Landeras-Bueno, E. Olmedillas, B. Laffey, K. Dobaczewska, Z. Mikulski, S. McArdle, S. R. Leist, K. Kim, R. S. Baric, E. Ollmann Saphire, A. Elong Ngono, S. Shresta, Human coronavirus OC43-elicited $CD4^+$ T cells protect against SARS-CoV-2 in HLA transgenic mice. *Nat. Commun.* **15**, 787 (2024).
46. A. H. A. Lavell, J. J. Sikkens, A. W. D. Edridge, K. van der Straten, F. Sechan, M. Oomen, D. T. P. Buis, M. Schinkel, J. A. Burger, M. Poniman, J. van Rijswijk, M. D. de Jong, G. J. de Bree, E. J. G. Peters, Y. M. Smulders, R. W. Sanders, M. J. van Gils, L. van der Hoek, M. K. Bomers, Recent infection with HCoV-OC43 may be associated with protection against SARS-CoV-2 infection. *iScience* **25**, 105105 (2022).
47. I. Saib, S. Aleisa, H. Ardah, E. Mahmoud, A. O. Alharbi, A. Alsaedy, S. Aljohani, A. Alshehri, N. K. Alharbi, M. Bosaeed, Non-SARS Non-MERS human coronaviruses: Clinical characteristics and outcome. *Pathogens* **10**, 1549 (2021).
48. J. Dworzański, B. Drop, E. Kliszczewska, M. Strycharz-Dudziak, M. Polz-Dacewicz, Prevalence of Epstein-Barr virus, human papillomavirus, cytomegalovirus and herpes simplex virus type 1 in patients with diabetes mellitus type 2 in south-eastern Poland. *PLOS ONE* **14**, e0222607 (2019).
49. E. A. Frick, V. Emilsson, T. Jonmundsson, A. E. Steindorsdottir, E. C. B. Johnson, R. Puerta, E. B. Dammer, A. Shantaraman, A. Cano, M. Boada, S. Valero, P. García-González, E. F. Gudmundsson, A. Gudjonsson, R. Pitts, X. Qiu, N. Finkel, J. J. Loureiro, A. P. Orth, N. T. Seyfried, A. I. Levey, A. Ruiz, T. Aspelund, L. L. Jennings, L. J. Launer, V. Gudmundsdottir, V. Gudnason, Serum proteomics reveal APOE-ε4-dependent and APOE-ε4-independent protein signatures in Alzheimer's disease. *Nat. Aging* **4**, 1446–1464 (2024).
50. H. Yousef, C. J. Czupalla, D. Lee, M. B. Chen, A. N. Burke, K. A. Zera, J. Zandstra, E. Berber, B. Lehallier, V. Mathur, R. V. Nair, L. N. Bonanno, A. C. Yang, T. Peterson, H. Hadeiba, T. Merkel, J. Körbelin, M. Schwaninger, M. S. Buckwalter, S. R. Quake, E. C. Butcher, T. Wyss-Coray, Aged blood impairs hippocampal neural precursor activity and activates microglia via brain endothelial cell VCAM1. *Nat. Med.* **25**, 988–1000 (2019).
51. K. Naruhashi, K. Kadomatsu, T. Igakura, Q. W. Fan, N. Kuno, H. Muramatsu, T. Miyauchi, T. Hasegawa, A. Itoh, T. Muramatsu, T. Nabeshima, Abnormalities of sensory and memory functions in mice lacking Bsg gene. *Biochem. Biophys. Res. Commun.* **236**, 733–737 (1997).
52. S. Zhou, H. Zhou, P. J. Walian, B. K. Jap, CD147 is a regulatory subunit of the γ-secretase complex in Alzheimer's disease amyloid β-peptide production. *Proc. Natl. Acad. Sci. U.S.A.* **102**, 7499–7504 (2005).
53. S. Wang, M. Mustafa, C. M. Yuede, S. V. Salazar, P. Kong, H. Long, M. Ward, O. Siddiqui, R. Paul, S. Gilfillan, A. Ibrahim, H. Rhinn, I. Tassi, A. Rosenthal, T. Schwabe, M. Colonna, Anti-human TREM2 induces microglia proliferation and reduces pathology in an Alzheimer's disease model. *J. Exp. Med.* **217**, (2020).
54. Y. Li, Z. Chen, Y. Gao, G. Pan, H. Zheng, Y. Zhang, H. Xu, G. Bu, H. Zheng, Synaptic adhesion molecule Pcdh-γC5 mediates synaptic dysfunction in Alzheimer's disease. *J. Neurosci.* **37**, 9259–9268 (2017).
55. K. Qin, L. Zhao, C. Gregory, A. Solanki, J. A. Mastrianni, "Dual disease" TgAD/GSS mice exhibit enhanced Alzheimer's disease pathology and reveal PrPC-dependent secretion of Aβ. *Sci. Rep.* **9**, 8524 (2019).
56. C. Chen, R. Kumbhar, H. Wang, X. Yang, K. Gadhave, C. Rastegar, Y. Kimura, A. Behensky, S. Kotha, G. Kuo, S. Katakam, D. Jeong, L. Wang, A. Wang, R. Chen, S. Zhang, L. Jin, C. J. Workman, D. A. A. Vignali, O. Pletinkova, H. Jia, W. Peng, D. W. Nauen, P. C. Wong, J. Redding-Ochoa, J. C. Troncoso, M. Ying, V. L. Dawson, T. M. Dawson, X. Mao, Lymphocyte-activation gene 3 facilitates pathological tau neuron-to-neuron transmission. *Adv. Sci.* **11**, e2303775 (2024).
57. N. W. Shock, R. C. Greulich, D. Aremberg, P. T. Costa, E. G. Lakatta, J. D. Tobin, *Normal Human Aging: The Baltimore Longitudinal Study of Aging*. (National Institutes of Health, 1984).
58. B. N. Ford, R. H. Yolken, F. B. Dickerson, T. K. Teague, M. R. Irwin, M. P. Paulus, J. Savitz, Reduced immunity to measles in adults with major depressive disorder. *Psychol. Med.* **49**, 243–249 (2019).
59. V. L. Nimgaonkar, R. H. Yolken, T. Wang, C.-C. H. Chang, L. McClain, E. McDade, B. E. Snitz, M. Ganguli, Temporal cognitive decline associated with exposure to infectious agents in a population-based, aging cohort. *Alzheimer Dis. Assoc. Disord.* **30**, 216–222 (2016).
60. S. M. Resnick, D. L. Pham, M. A. Kraut, A. B. Zonderman, C. Davatzikos, Longitudinal magnetic resonance imaging studies of older adults: A shrinking brain. *J. Neurosci.* **23**, 3295–3301 (2003).
61. J. Doshi, G. Erus, Y. Ou, S. M. Resnick, R. C. Gur, R. E. Gur, T. D. Satterthwaite, S. Furth, C. Davatzikos, Alzheimer's Neuroimaging Initiative, MUSE: Multi-atlas region segmentation utilizing ensembles of registration algorithms and parameters, and locally optimal atlas selection. *Neuroimage* **127**, 186–195 (2016).
62. M. Bilgel, Y. An, K. A. Walker, A. R. Moghekar, N. J. Ashton, P. R. Kac, T. K. Karikari, K. Blennow, H. Zetterberg, B. M. Jedynak, M. Thambisetty, L. Ferrucci, S. M. Resnick, Longitudinal changes in Alzheimer's-related plasma biomarkers and brain amyloid. *Alzheimers Dement.* **19**, 4335–4345 (2023).
63. M. Bilgel, Y. An, Y. Zhou, D. F. Wong, J. L. Prince, L. Ferrucci, S. M. Resnick, Individual estimates of age at detectable amyloid onset for risk factor assessment. *Alzheimers Dement.* **12**, 373–379 (2016).
64. M. Schöll, S. N. Lockhart, D. R. Schonhaut, J. P. O'Neil, M. Janabi, R. Ossenkoppele, S. L. Baker, J. W. Vogel, J. Faria, H. D. Schwimmer, G. D. Rabinovici, W. J. Jagust, PET imaging of Tau deposition in the aging human brain. *Neuron* **89**, 971–982 (2016).
65. M. Bilgel, D. F. Wong, A. R. Moghekar, L. Ferrucci, S. M. Resnick, the Alzheimer's Disease Neuroimaging Initiative, Causal links among amyloid, tau, and neurodegeneration. *Brain Commun.* **4**, fcac193 (2022).
66. S. L. Seliger, C. R. Wendell, S. R. Waldstein, L. Ferrucci, A. B. Zonderman, Renal function and long-term decline in cognitive function: The Baltimore Longitudinal Study of Aging. *Am. J. Nephrol.* **41**, 305–312 (2015).
67. T. K. Karikari, T. A. Pascoal, N. J. Ashton, S. Janelidze, A. L. Benedet, J. L. Rodriguez, M. Chamoun, M. Savard, M. S. Kang, J. Therriault, M. Schöll, G. Massarweh, J.-P. Soucy, K. Höglund, G. Brinkmalm, N. Mattsson, S. Palmqvist, S. Gauthier, E. Stomrud, H. Zetterberg, O. Hansson, P. Rosa-Neto, K. Blennow, Blood phosphorylated tau 181 as a biomarker for Alzheimer's disease: A diagnostic performance and prediction modelling study using data from four prospective cohorts. *Lancet Neurol.* **19**, 422–433 (2020).
68. J. Candia, G. N. Daya, T. Tanaka, L. Ferrucci, K. A. Walker, Assessment of variability in the plasma 7k SomaScan proteomics assay. *Sci. Rep.* **12**, 17147 (2022).
69. J. D. Wright, A. R. Folsom, J. Coresh, A. R. Sharrett, D. Couper, L. E. Wagenknecht, T. H. Mosley Jr., C. M. Ballantyne, E. A. Boerwinkle, W. D. Rosamond, G. Heiss, The ARIC (Atherosclerosis Risk In Communities) study: JACC focus seminar 3/8. *J. Am. Coll. Cardiol.* **77**, 2939–2959 (2021).
70. K. A. Walker, J. Chen, J. Zhang, M. Fornage, Y. Yang, L. Zhou, M. E. Grams, A. Tin, N. Daya, R. C. Hoogeveen, A. Wu, K. J. Sullivan, P. Ganz, S. L. Zeger, E. F. Gudmundsson, V. Emilsson, L. J. Launer, L. L. Jennings, V. Gudnason, N. Chatterjee, R. F. Gottesman, T. H. Mosley, E. Boerwinkle, C. M. Ballantyne, J. Coresh, Large-scale plasma proteomic analysis identifies proteins and pathways associated with dementia risk. *Nat. Aging* **1**, 473–489 (2021).
71. R. F. Gottesman, A. L. Schneider, Y. Zhou, X. Chen, E. Green, N. Gupta, D. S. Knopman, A. Mintz, A. Rahmim, A. R. Sharrett, L. E. Wagenknecht, D. F. Wong, T. H. Mosley Jr., The ARIC-PET amyloid imaging study: Brain amyloid differences by age, race, sex, and APOE. *Neurology* **87**, 473–480 (2016).
72. D. S. Knopman, R. F. Gottesman, A. R. Sharrett, L. M. Wruck, B. G. Windham, L. Coker, A. L. Schneider, S. Hengrui, A. Alonso, J. Coresh, M. S. Albert, T. H. Mosley Jr., Mild cognitive impairment and dementia prevalence: The Atherosclerosis Risk in Communities Neurocognitive Study (ARIC-NCS). *Alzheimers Dement.* **2**, 1–11 (2016).
73. O. Murrin, N. Mounier, B. Voller, L. Tata, C. Gallego-Moll, A. Roso-Llorach, L. A. Carrasco-Ribelles, C. Fox, L. M. Allan, R. M. Woodward, X. Liang, J. M. Valderas, S. M. Khalid, F. Dudbridge, S. E. Lamb, M. Mancini, L. Farmer, K. Boddy, J. Bowden, D. Melzer, T. M. Frayling, J. A. H. Masoli, L. C. Pilling, C. Violán, J. Delgado, A systematic analysis of the contribution of genetics to multimorbidity and comparisons with primary care data. *EBioMedicine* **113**, 105584 (2025).
74. T. Waterboer, P. Sehr, K. M. Michael, S. Franceschi, J. D. Nieland, T. O. Joos, M. F. Templin, M. Pawlita, Multiplex human papillomavirus serology based on in situ-purified glutathione s-transferase fusion proteins. *Clin. Chem.* **51**, 1845–1853 (2005).
75. D. A. Bennett, A. S. Buchman, P. A. Boyle, L. L. Barnes, R. S. Wilson, J. A. Schneider, Religious orders study and rush memory and aging project. *J. Alzheimers Dis.* **64**, S161–s189 (2018).
76. H. S.-H. Oh, D. Y. Urey, L. Karlsson, Z. Zhu, Y. Shen, A. Farinas, J. Timsina, I. H. Guldner, N. Morshed, C. Yang, D. Western, M. Ali, Y. Le Guen, A. Trelle, S.-K. Herukka, T. Rauamaa, M. Hiltunen, A. Lipponen, A. J. Luikku, K. L. Poston, E. Mormino, A. D. Wagner, E. N. Wilson, D. Channappa, V. Leinonen, B. Stevens, A. J. Ehrenberg, H. Zetterberg, D. A. Bennett, N. Franzmeier, O. Hansson, C. Cruchaga, T. Wyss-Coray, Synapse protein signatures in cerebrospinal fluid and plasma predict cognitive maintenance versus decline in Alzheimer's disease. bioRxiv 2024.07.22.604680 [Preprint] (2024). https://doi.org/10.1101/2024.07.22.604680.
77. Z. Yang, J. Wen, G. Erus, S. T. Govindarajan, R. Melhem, E. Mamourian, Y. Cui, D. Srinivasan, A. Abdulkadir, P. Parmpi, K. Wittfeld, H. J. Grabe, R. Bülow, S. Frenzel, D. Tosun, M. Bilgel, Y. An, D. Yi, D. S. Marcus, P. LaMontagne, T. L. S. Benzinger, S. R. Heckbert, T. R. Austin, S. R. Waldstein, M. K. Evans, A. B. Zonderman, L. J. Launer, A. Sotiras, M. A. Espeland, C. L. Masters, P. Maruff, J. Fripp, A. W. Toga, S. O'Bryant, M. M. Chakravarty, S. Villeneuve, S. C. Johnson, J. C. Morris, M. S. Albert, K. Yaffe, H. Völzke, L. Ferrucci, R. Nick Bryan, R. T. Shinohara, Y. Fan, M. Habes, P. A. Lalousis, N. Koutsouleris, D. A. Wolk, S. M. Resnick, H. Shou, I. M. Nasrallah, C. Davatzikos, Brain aging patterns in a large and diverse cohort of 49,482 individuals. *Nat. Med.* **30**, 3015–3026 (2024).
78. J. Wen, Z. Yang, I. M. Nasrallah, Y. Cui, G. Erus, D. Srinivasan, A. Abdulkadir, E. Mamourian, G. Hwang, A. Singh, M. Bergman, J. Bao, E. Varol, Z. Zhou, A. Boquet-Pujadas, J. Chen,

A. W. Toga, A. J. Saykin, T. J. Hohman, P. M. Thompson, S. Villeneuve, R. Gollub, A. Sotiras, K. Wittfeld, H. J. Grabe, D. Tosun, M. Bilgel, Y. An, D. S. Marcus, P. LaMontagne, T. L. Benzinger, S. R. Heckbert, T. R. Austin, L. J. Launer, M. Espeland, C. L. Masters, P. Maruff, J. Fripp, S. C. Johnson, J. C. Morris, M. S. Albert, R. N. Bryan, S. M. Resnick, L. Ferrucci, Y. Fan, M. Habes, D. Wolk, L. Shen, H. Shou, C. Davatzikos, Genetic and clinical correlates of two neuroanatomical AI dimensions in the Alzheimer's disease continuum. *Transl. Psychiatry* **14**, 420 (2024).

79. A. Krämer, J. Green, J. Pollard Jr., S. Tugendreich, Causal analysis approaches in ingenuity pathway analysis. *Bioinformatics* **30**, 523–530 (2014).
80. E. Y. Chen, C. M. Tan, Y. Kou, Q. Duan, Z. Wang, G. V. Meirelles, N. R. Clark, A. Ma'ayan, Enrichr: Interactive and collaborative HTML5 gene list enrichment analysis tool. *BMC Bioinformatics* **14**, 128 (2013).
81. O. Franzén, L. M. Gan, J. L. M. Björkegren, PanglaoDB: A web server for exploration of mouse and human single-cell RNA sequencing data. *Database* **2019**, baz046 (2019).
82. H. S.-H. Oh, J. Rutledge, D. Nachun, R. Pálovics, O. Abiose, P. Moran-Losada, D. Channappa, D. Y. Urey, K. Kim, Y. J. Sung, L. Wang, J. Timsina, D. Western, M. Liu, P. Kohlfeld, J. Budde, E. N. Wilson, Y. Guen, T. M. Maurer, M. Haney, A. C. Yang, Z. He, M. D. Greicius, K. I. Andreasson, S. Sathyan, E. F. Weiss, S. Milman, N. Barzilai, C. Cruchaga, A. D. Wagner, E. Mormino, B. Lehallier, V. W. Henderson, F. M. Longo, S. B. Montgomery, T. Wyss-Coray, Organ aging signatures in the plasma proteome track health and disease. *Nature* **624**, 164–172 (2023).
83. A. Franceschini, D. Szklarczyk, S. Frankild, M. Kuhn, M. Simonovic, A. Roth, J. Lin, P. Minguez, P. Bork, C. von Mering, L. J. Jensen, STRING v9.1: Protein-protein interaction networks, with increased coverage and integration. *Nucleic Acids Res.* **41**, D808–D815 (2013).
84. H. Mathys, J. Davila-Velderrain, Z. Peng, F. Gao, S. Mohammadi, J. Z. Young, M. Menon, L. He, F. Abdurrob, X. Jiang, A. J. Martorell, R. M. Ransohoff, B. P. Hafler, D. A. Bennett, M. Kellis, L.-H. Tsai, Single-cell transcriptomic analysis of Alzheimer's disease. *Nature* **570**, 332–337 (2019).
85. A. C. Yang, R. T. Vest, F. Kern, D. P. Lee, M. Agam, C. A. Maat, P. M. Losada, M. B. Chen, N. Schaum, N. Khoury, A. Toland, K. Calcuttawala, H. Shin, R. Pálovics, A. Shin, E. Y. Wang, J. Luo, D. Gate, W. J. Schulz-Schaeffer, P. Chu, J. A. Siegenthaler, M. W. McNerney, A. Keller, T. Wyss-Coray, A human brain vascular atlas reveals diverse mediators of Alzheimer's risk. *Nature* **603**, 885–892 (2022).
86. D. K. Kim, D. Han, J. Park, H. Choi, J.-C. Park, M.-Y. Cha, J. Woo, M. S. Byun, D. Y. Lee, Y. Kim, I. Mook-Jung, Deep proteome profiling of the hippocampus in the 5XFAD mouse model reveals biological process alterations and a novel biomarker of Alzheimer's disease. *Exp. Mol. Med.* **51**, 1–17 (2019).
87. A. Sierksma, A. Lu, R. Mancuso, N. Fattorelli, N. Thrupp, E. Salta, J. Zoco, D. Blum, L. Buée, B. De Strooper, M. Fiers, Novel Alzheimer risk genes determine the microglia response to amyloid-β but not to TAU pathology. *EMBO Mol. Med.* **12**, e10606 (2020).
88. M. R. Duggan, G. T. Gomez, C. M. Joynes, M. Bilgel, J. Chen, N. Fattorelli, T. J. Hohman, R. Mancuso, J. Cordon, T. Castellano, M. E. I. Koran, J. Candia, A. Lewis, A. Moghekar, N. J. Ashton, P. R. Kac, T. K. Karikari, K. Blennow, H. Zetterberg, A. Martinez-Muriana, B. De Strooper, M. Thambisetty, L. Ferrucci, R. F. Gottesman, J. Coresh, S. M. Resnick, K. A. Walker, Proteome-wide analysis identifies plasma immune regulators of amyloid-beta progression. *Brain Behav. Immun.* **120**, 604–619 (2024).

Acknowledgments: We thank the BLSA participants and staff for participation and continued dedication, as well as the staff and participants of the ARIC study for important contributions. We also thank A. Nath for feedback on an initial draft of the manuscript. **Funding:** This research was supported by the Intramural Research Program (IRP) of the NIH, National Institute on Aging (NIA), and The Stanley Medical Research Institute. ARIC is carried out as a collaborative study supported by NHLBI contracts (75N92022D00001, 75N92022D00002, 75N92022D00003, 75N92022D00004, and 75N92022D00005). The ARIC Neurocognitive Study was additionally supported by U01HL096812, U01HL096814, U01HL096899, U01HL096902, and U01HL096917 from the NIH [NHLBI, NIA, National Institute of Neurological Disorders and Stroke (NINDS), and National Institute on Deafness and Other Communication Disorders (NIDCD)]. The ARIC-PET study was supported by the NIA (R01AG040282). A.M. was supported by the NIA (U19AG033655 and P30AG066507). H.Z. is a Wallenberg Scholar and a Distinguished Professor at the Swedish Research Council supported by grants from the Swedish Research Council (nos. 2023-00356, 2022-01018, and 2019-02397), the European Union's Horizon Europe research and innovation program under grant agreement no. 101053962, Swedish State Support for Clinical Research (no. ALFGBG-71320), the Alzheimer Drug Discovery Foundation (ADDF), USA (no. 201809-2016862), the AD Strategic Fund and the Alzheimer's Association (nos. ADSF-21-831376-C, ADSF-21-831381-C, ADSF-21-831377-C, and ADSF-24-1284328-C), the European Partnership on Metrology, cofinanced from the European Union's Horizon Europe Research and Innovation Programme and the Participating States (NEuroBioStand, no. 22HLT07), the Bluefield Project, Cure Alzheimer's Fund, the Olav Thon Foundation, the Erling-Persson Family Foundation, Familjen Rönströms Stiftelse, Stiftelsen för Gamla Tjänarinnor, Hjärnfonden, Sweden (no. FO2022-0270), the European Union's Horizon 2020 research and innovation program under the Marie Skłodowska-Curie grant agreement no. 860197 (MIRIADE), the European Union Joint Programme–Neurodegenerative Disease Research (JPND2021-00694), the National Institute for Health and Care Research University College London Hospitals Biomedical Research Centre, and the UK Dementia Research Institute at UCL (UKDRI-1003). T.K.K. was supported by grants R01AG083874-01, U24AG082930-01, P30AG066468, RF1AG052525-01A1, R01AG053952-05, R37AG023651-17, RF1AG025516-12A1, R01AG073267-02, R01AG075336-01, R01AG072641-02, and P01AG025204-16 from the NIH, the Swedish Research Council (2021-03244), the Alzheimer's Association (AARF-21-850325), the Swedish Alzheimer Foundation, the Aina Wallströms and Mary-Ann Sjöblom foundation, and the Emil and Wera Cornell foundation. K.B. was supported by the Swedish Research Council (2017-00915 and 2022-00732), the Swedish Alzheimer Foundation (AF-930351, AF-939721, and AF-968270), the Swedish Brain Foundation (FO2017-0243 and ALZ2022-0006), the Swedish state under the agreement between the Swedish government and the County Councils, the ALF agreement (ALFGBG-715986 and ALFGBG-965240), the European Union Joint Program for Neurodegenerative Disorders (JPND2019-466-236), the Alzheimer's Association 2021 Zenith Award (ZEN-21-848495), and the Alzheimer's Association 2022–2025 Grant (SG-23-1038904 QC). A.P.S. and B.S.M. were supported by the NIA (R01AG075996). R.F.G. was supported by the NINDS IRP. C.D. was supported by RF1AG054409. Data from the UKB were used via application 83534. ROSMAP is supported by P30AG10161, P30AG72975, R01AG15819, R01AG17917, U01AG46152, and U01AG61356. **Author contributions:** M.R.D. conceived and designed the study. M.R.D. conducted primary statistical analysis and wrote the first draft of the paper. S.Y. provided technical assistance. G.T.G., Y.C., A.W.C., J.Ca., Z.Y., J.W., G.E., S.M.D., D.Z., Q.T., J.Ch., M.B., A.L., A.M., N.J.A., P.R.K., T.K.K., K.B., H.Z., A.P.S., B.S.M., L.D., and T.J.H. conducted supplementary statistical analyses, curated data, and/or provided scientific expertise. R.F.G., C.D., D.A.B., J.Co., L.F., S.M.R., R.Y., and K.A.W. obtained funding. M.R.D., R.Y., and K.A.W. supervised the study. M.R.D., S.Y., G.T.G., Y.C., A.W.C., J.Ch., Z.Y., J.W., G.E., S.M.D., D.Z., Q.T., J.Ca., M.B., A.L., A.M., N.J.A., P.R.K., T.K.K., K.B., H.Z., B.S.M., A.P.S., L.D., T.J.H., R.F.G., C.D., D.A.B., J.Co., L.F., S.M.R., R.Y., and K.A.W. contributed to revisions of the paper and approved the final version as submitted. **Competing interests:** K.A.W. is an associate editor at Alzheimer's & Dementia, a member of the Editorial Board of Annals of Clinical and Translational Neurology, and on the board of directors of the National Academy of Neuropsychology. H.Z. has served at scientific advisory boards and/or as a consultant for Abbvie, Acumen, Alector, Alzinova, ALZPath, Amylyx, Annexon, Apellis, Artery Therapeutics, AZTherapies, Cognito Therapeutics, CogRx, Denali, Eisai, LabCorp, Merry Life, Nervgen, Novo Nordisk, Optoceutics, Passage Bio, Pinteon Therapeutics, Prothena, Red Abbey Labs, reMYND, Roche, Samumed, Siemens Healthineers, Triplet Therapeutics, and Wave; has given lectures in symposia sponsored by Alzecure, Biogen, Cellectricon, Fujirebio, Lilly, Novo Nordisk, and Roche; and is a cofounder of Brain Biomarker Solutions in Gothenburg AB (BBS), which is a part of the GU Ventures Incubator Program (outside submitted work). K.B. has served as a consultant and at advisory boards for Acumen, ALZPath, BioArctic, Biogen, Eisai, Lilly, Moleac Pte. Ltd., Novartis, Ono Pharma, Prothena, Roche Diagnostics, and Siemens Healthineers; has served at data monitoring committees for Julius Clinical and Novartis; has given lectures, produced educational materials, and participated in educational programs for AC Immune, Biogen, Celdara Medical, Eisai, and Roche Diagnostics; and is a cofounder of Brain Biomarker Solutions in Gothenburg AB, which is a part of the GU Ventures Incubator Program, outside the work presented in this paper. A.P.S. received payment for serving as a consultant for Merck, received honoraria from Springer Nature Switzerland AG for guest editing special issues of Current Sleep Medicine Reports, and is a paid consultant to Sequoia Neurovitality, BellSant Inc., and Amissa Inc. T.K.K. has consulted for Quanterix Corp., SpearBio Inc., and Neurogen Biomarking LLC. and has received honoraria from the NIH for study section membership and honoraria for speaker/grant review engagements from the University of Pennsylvania, University of Wisconsin-Madison, Advent Health, Brain Health conference, Barcelona-Pittsburgh conference, and CQDM Canada, all outside of the submitted work. T.K.K has received blood biomarker data on defined research cohorts from Janssen and Alamar Biosciences for independent analysis and publication, with no financial incentive and/or research funding included. T.K.K is an inventor on patent no. WO2020193500A1 and patent application nos. 2450702-2, 63/693,956, 63/679,361, and 63/672,952. T.J.H. is on the scientific advisory board for Vivid Genomics, the deputy editor for Alzheimer's & Dementia: Translational Research and Clinical Intervention, and the senior associate editor for Alzheimer's & Dementia. All other coauthors report no relevant conflicts of interest. **Data and materials availability:** All data generated in the present study are included in this article, in an online public repository, or available upon reasonable request from an independent steering committee. Participant-level demographic, clinical, and proteomic data from the BLSA cannot be deposited in a public database based on prior participant consent and data sharing restrictions. However, deidentified BLSA data not published within this article may be shared upon request with qualified investigators. For participants in the Global Neurodegeneration Proteomics Consortium (www.neuroproteome.org), BLSA proteomic data are available via the Alzheimer's Disease Data Initiative (www.alzheimersdata.org/). For investigators who are not part of this consortium and interested in requesting access to BLSA proteomics data for purposes of reproducibility, researchers should submit a preanalysis plan for approval (https://blsa.nia.nih.gov/how-apply). ARIC proteomic data (accession number: HLB00020023a) are available through the National Heart Lung and Blood Institutes Biologic Specimen and Data Repository Information Coordinating Center (https://biolincc.nhlbi.nih.gov/studies/aric).

Participant-level demographic, clinical, and proteomic data may be partially restricted on the basis of prior participant consent, and data sharing restrictions may also be applied to ensure consistency with confidentiality or privacy laws and considerations (https://sites.cscc.unc.edu/aric/). Requests for clinical or proteomic data subject to these constraints may be submitted to the ARIC Steering Committee and will be reviewed to ensure that data can be shared without compromising participant confidentiality or breaching intellectual property restrictions. Data, protocols, and other metadata of the UKB are available to the scientific community upon request in accordance with the UKB data sharing policy (www.ukbiobank.ac.uk/enable-your-research/apply-for-access). ROSMAP resources are available upon request at www.radc.rush.edu and www.synapse.org/Synapse:syn3219045 . No original code was developed for this study. Analyses used publicly available R packages, including stats (4.4), tidyverse (2.0), nlme (3.1), TwoSampleMR (0.6.6), and ggplot2 (3.5), with basic functions (e.g., lm, full_join, mr, geom_point, etc.).

Submitted 8 October 2024
Accepted 25 April 2025
Published 30 May 2025
10.1126/sciadv.adt7176